Dynamical edge-vortex excitations:
Injection, braiding and detection

by

I.M. Flór

to obtain the degree of Master of Science in
Applied Physics and Applied Mathematics
at Delft University of Technology,
to be defended publicly on Monday, February 13th, 2023 at 13:00.

Student number:	4486870,	
Project duration:	February 7, 2022 – February 7, 2023,	
Thesis committee:	Prof. C.W.J. Beenakker,	Leiden supervisor,
	Dr. J.L.A. Dubbeldam,	TU Delft supervisor,
	Dr. A.R. Akhmerov,	TU Delft supervisor,
	Dr. J. Thies,	TU Delft examiner,
Groups:	Theoretical Nanophysics,	Instituut Lorentz Leiden
	Mathematical Physics,	Delft Institute of Applied Mathematics

TU Delft

Abstract

The detection of non-Abelian exchange statistics is an open challenge which holds important promises for the advent of topological quantum computation. A recent work proposes to rely on the edges to reveal the braiding statistics of non-Abelian anyons in the bulk, in an entirely deterministic dynamical process. A time-dependent gap in a Josephson junction couples two co-propagating Majorana fermions, and as the gap closes, a pair of edge-vortices is injected into the edges. Because these defects have the same non-Abelian statistics, they are braided with vortices in the bulk. Conveniently, the fusion of the edge-vortices results in a quantized unit of charge at the exit. However, this process is so far only predicted in the adiabatic limit. In this work, this assumption is relaxed by means of a full many-body evolution of the superconducting ground state in the Bogoliubov-de-Gennes formalism. Beyond revealing the collective nature of the edge-vortex excitation, we demonstrate that the quantization of charge still holds if the system does not return to the ground state. Furthermore, the effect of path length difference between the edge-vortices confirms the theoretical predictions done in another work on the subject. At fast injections, we reveal weak oscillations in current contributed by the bound states in the junction which average to zero and are removed in the short junction limit. This work is concluded with a preliminary evaluation of the many-body parity operator, which indicates that the edge-vortex may encode the parity of the bulk vortices. This opens the possibility for sequential qubit manipulations on the edge-vortex.

Acknowledgements

I would like to thank Álvaro and Gal for their invaluable help and for the enlightening discussions throughout the project. I would like to thank Carlo for his guidance and generosity, and Johan and Anton for keeping an eye on the project throughout the year from Delft. Finally, I would like to thank Jonas for taking the time to participate in the assessment.

Contents

■ Chapter I
Introduction

1. Background

The existence of non-Abelian anyons underlies the formulation of topological quantum information processing [1–3]. The adiabatic motion of non-Abelian anyons results in unitary operations between them, which is in particular true when they are exchanged. This is known as braiding. Strikingly, transformations achieved by braiding naturally lend themselves to a number of quantum computing operations on the topologically protected qubit [1]. Majorana zero-modes (MZMs) are zero-dimensional midgap states which belong to a particular class of non-Abelian anyons: one pair of MZMs can encode a qubit as it may or may not share an unpaired fermion [4].

While experimental efforts are at the stage of detection of MZMs [5–7], a number of theoretical proposals have been formulated for the detection of their braiding. Because MZMs arise at the ends of one-dimensional topological superconductors or at the core of vortices in p-wave superconductors [8–11], mobile braiding schemes require setting vortices in motion, which is a difficult task [12]. Therefore, most efforts have been focused on immobile braiding schemes in 1D nanowire systems using tri-junction configurations [2, 13–17]. However, a recent study [18] proposes a strategy to achieve mobile braiding: by injecting vortex-like defects through a Josephson junction into the chiral edge modes – referred to as edge-vortices –, the latter can be braided with static vortices in the bulk because they share the same exchange statistics [19]; the pair of edge-vortices thus encodes a flying qubit which may exchange parity with the bulk vortices. Ramifications of this proposal have been studied as a result [20–23].

Most remarkably, the fused edge-vortices produce a *quantized* unit of charge at their readout depending on whether they were braided with bulk vortices. The theory relies on the central assumption that a time-dependent gap in the junction is inverted adiabatically, so that the process returns to the ground state after the evolution. In this thesis, this assumption is addressed by means of a dynamical simulation in the Bogoliubov-de-Gennes formalism, of a system which satisfies the proposal. In particular, one may question the role of Andreev bound states in the Josephson junction, known for leaking charge into fermionic edge states when the junction is excited [24, 25] or interfering with the detection of MZMs in a number of different proposals [26–29]. Furthermore, we perform preliminary calculations of the many-body parity operator dynamically, which allows us to assess whether the edge-vortex is a good qubit.

In the remainder of this chapter, we introduce the notions of braiding in more

detail. In Ch. II the relevant results obtained in previous works is summarized. A model for the Hamiltonian of the system is developed in Ch. III and followed by the numerical model for the time-dependent system in Ch. IV. After treating the description of time-evolved ground state expectation values in Ch. V, we assess the quantization of charge dynamically. Before concluding in Ch. VIII, we present the results on the parity of the edge-vortex in Ch. VII.

2. Injection and braiding of edge-vortices

2.1. Parity qubits and braiding of Majorana zero-modes

Before a formal treatment in the next chapter, we introduce the notions of particle-hole symmetry, Majorana zero-modes and braiding in general terms. This serves as a background to introduce the edge-vortex braiding setup in the next subsection. For a detailed overview we refer to the reviews in Refs. [1–3].

Particle-hole symmetry.— Superconductivity in the mean-field BCS theory is described with the potential $\Delta = |\Delta|(\mathbf{r})e^{i\phi(\mathbf{r})}$ which couples pairs of electrons. In the Bogoliubov-de-Gennes formalism, this is equivalently described as a coupling between an electron and a hole. The allowed excitations of the superconducting ground state which results from the presence of the gap Δ are called Bogoliubov quasiparticles and satisfy particle-hole symmetry. If $\gamma^\dagger$ (γ) denotes the creation (annihilation) operator for such an excitation, then this condition is:

$$\gamma^\dagger(E) = \gamma(-E).$$

Crucially, given a ground state of N electrons, the Bogoliubov excitation does not necessarily change the number of electrons to $N \pm 1$; it may also change it to e.g. $N + 3$. Nevertheless, the number of electrons is only allowed to change by an odd number of electrons to $N \pm k$ with k odd. We say the Bogoliubov excitation has a well defined contribution to the ground state parity.

Majorana zero-modes.— If one finds a state which exists at $E = 0$, then this level must satisfy $\gamma^\dagger = \gamma$ by particle-hole symmetry. The operator is therefore real and corresponds with a quasi-particle which is equal to its anti-particle known as a Majorana fermion. The latter obeys unusual anti-commutation relations as $\gamma_n\gamma_m + \gamma_n\gamma_m = 2\delta_{nm}$ for two Majorana operators γ_n, γ_m [3]. In particular, a Majorana zero-mode is the state which arises when a Majorana fermion is unpaired into two zero-dimensional states [2]. Note that by definition, the MZM is in a superposition of even and odd parity contributions to the ground state. If such a state exists, then it forms a qubit of electron number parity which is protected from other states by particle-hole symmetry. Concretely, given a fermion $\psi^\dagger$ (odd parity) or ψ (even parity) it can be unpaired into two zero-modes γ_1 and γ_2 such that its operators are:

$$\psi = \gamma_1 + i\gamma_2 \quad \text{and} \quad \psi^\dagger = \gamma_1 - i\gamma_2$$

so we label the state of even parity (+) and odd parity (−) in the remainder.

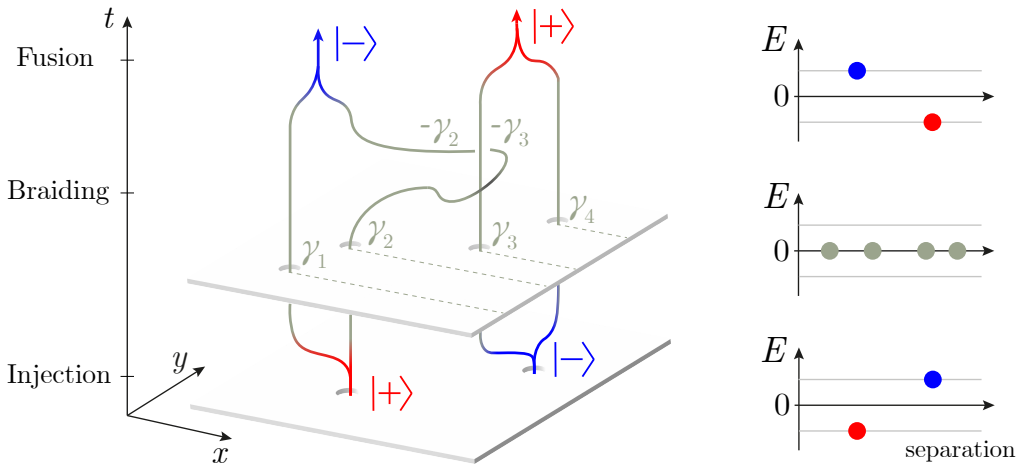

Figure I.1: Illustration of an injection, braiding and fusion process which implements an exchange operation σ_x on the parity qubit degree of freedom; illustration based on Ref. [2]. The world lines are indicated with solid curves. The braiding process can be though of in terms of branch cuts in the phase of the superconductor (dashed lines). The energy levels throughout the process are shown on the right.

Braiding statistics.— In the fermionic expressions above it is clear that if $\gamma_2 \to -\gamma_2$, this will induce $\psi \to \psi^\dagger$. This is a change in parity. It turns out that a change in the sign of a MZM can be achieved by a 2π phase increase of the pairing potential Δ, i.e. an adiabatic transformation $\phi \to \phi + \varphi$ results in a MZM gaining a phase $\gamma \to e^{i\varphi/2}\gamma$ [30]. This is the root of their non-Abelian anyonic nature. To illustrate this let us consider two fermions – say one $\psi = \gamma_1 + i\gamma_2$ with even parity $(+)$ at energy $-\varepsilon$ and the other one $\psi^\dagger = \gamma_3 - i\gamma_4$ with odd parity $(-)$ at $+\varepsilon$. Then suppose there is a mechanism by which the fermions are unpaired into zero modes back in the ground state manifold $E = 0$ as shown in Fig. I.1. That mechanism here is the presence of vortices: two vortices will "split" the fermion into two zero modes which bind to the cores of the vortices. If γ_2 performs a closed loop in space around γ_3, they will mutually *induce a phase sign* on each other. When γ_1 and γ_2 fuse again into their fermionic state, they now correspond to the state of *opposite parity* because of that sign difference. This exchange is entirely non-local since it happens through the phase of the superconductor, so that the vortices never came near each other. It is possible to visualize this: the vortex corresponds with a phase winding of 2π which means a π phase for the MZM. The π jump can be seen as a discontinuity which occurs at the branch-cut of the superconducting phase ϕ. It naturally follows that when two branch-cuts cross each other, this will cancel the π discontinuity which occurs there. In Fig. I.1 the locations of the branch cuts in the phase around the vortices are shown so that the entire braiding process can be thought of in terms of crossing branch-cuts. The resulting braiding operation between γ_2 and γ_3 can be described in terms of the unitary transformation [30]:

$$\hat{U}_{23} = e^{\frac{\pi}{4}\gamma_2\gamma_3} = \frac{1}{\sqrt{2}}(I + \gamma_2\gamma_3).$$

2.2. Deterministic injection and braiding of edge-vortices

Edge-vortices.— The local phase $\phi(\mathbf{r})$ of the superconductor also affects a fermion that exists on its boundaries. If the edge state of a superconductor is a Majorana fermion $\chi(x)$ then a 2π increase of the phase in the superconductor results in a π increase of the Majorana wave function on the edge. The resulting π jump on the edge is the edge-vortex. In particular, if the 2π phase increase is due to the presence of a vortex, then the edge and the vortex share a state of parity which imposes the existence of an edge-vortex. Given a closed path of length L parametrized by $x \in [0, L)$ and denoting the number of vortices inside the superconductor by N_{vortex}, this results in anti-periodic boundary conditions on the Majorana fermion at the edge [19]:

$$\chi(x = 0) = (-1)^{N_{\text{vortex}}+1}\chi(x = L).$$

This local boundary condition is analogous to the branch-cut of the MZMs introduced in the previous subsection and it therefore follows the same braiding statistics.

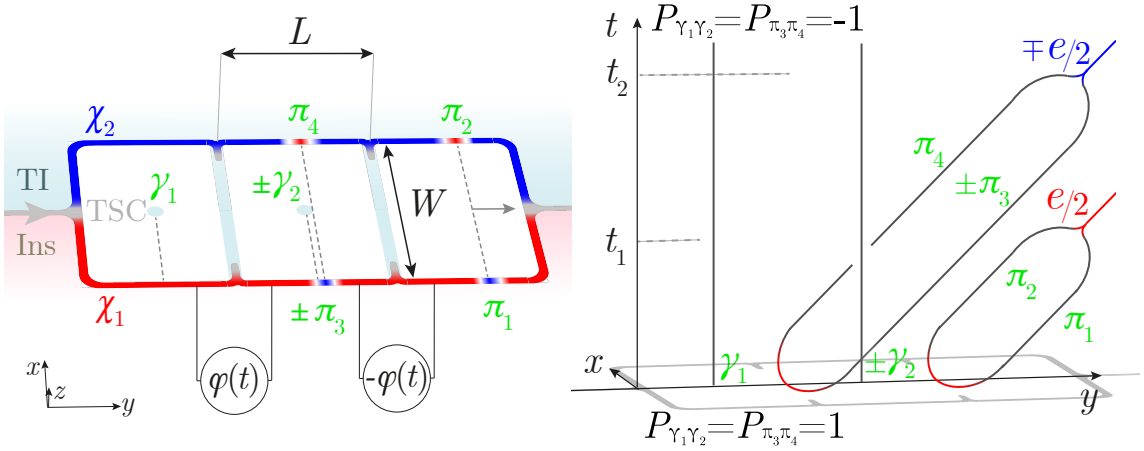

Figure I.2: (Left) Setup representation. MZMs with their branch-cuts (dashed lines), and Majorana fermions χ_1, χ_2 (red, blue) such that the pair π_3, π_4 is braided with the pair γ_1, γ_2 after their injection in the junction. (Right) Spacetime diagram of the braiding scheme in the setup showing charge and parity with $(-)$ and without $(+)$ vortices.

Injection and braiding setup.— We now consider the case where Josephson junctions are used to create a 2π phase increase of the superconducting phase [29, 31–33]. Consider three superconductors separated by two Josephson junctions such that the phase in the middle superconductor differs by a phase $\varphi(t)$ with the other superconductors, as shown in Fig. I.2. Then, suppose that two co-propagating Majorana fermions $\chi_i(y - vt)$, $i \in \{1, 2\}$ with constant velocity v enter the middle superconductor at its bottom and top edges respectively. This can be realized at the interface of a topological superconductor with a trivial insulator and a topological insulator [34] as shown in Fig.I.2. Following a 2π increase of $\varphi(t)$, the Majorana fermions experience the expected phase flip $\chi_i(y - vt) \to e^{\pm i\pi}\chi_i(y - vt)$ at each Josephson junction, say during a characteristic time t_{inj}. More precisely, this phase flip occurs exactly in the junction: at $\varphi = 0$ a small gap Δ_0 separates the edges modes at opposite sides of the junction, and this gap closes at $\varphi = \pi$ and inverts following $\Delta_0 \cos(\varphi(t)/2)$. In analogy with the Kitaev chain [10], this gap inversion has to produce unpaired fermions in the junction which propagate as phase defects

on the edges (the edge-vortices), which travel towards the exit with a velocity v. The gap Δ_0 is shown in the band structure in Fig. I.3. The resulting is the creation of four co-propagating edge-vortices: two at the front junction π_1, π_2 and two at the back junction π_3, π_4. Note that since the Josephson pump cannot create an unpaired fermion, the parity values are $P_{34} = i\pi_3\pi_4 = 1$ is even and so is $P_{12} = i\pi_1\pi_2 = 1$ [20]. At their fusions, the zero modes produce a charge $+e/2$ and $-e/2$ respectively, thereby resulting in a net *zero charge* transfer. However, if a vortex is present in the bulk, the second pair π_3, π_4 collectively crosses the branch cut of the bulk vortex γ_2. Therefore, the pair π_3, π_4 changes sign relative to the pair γ_1, γ_2. The braiding scheme is shown in the spacetime diagram in Fig. I.2. When the edge-vortices fuse, both pairs now produce an $e/2$ charge carrying defect so that the net transferred charge is that of an electron e.

3. Dynamical considerations

The braiding process of edge-vortices was predicted in an adiabatic approximation [18, 22]. In the dynamical picture, the injection of edge-vortices is entirely governed by the Josephson junctions. If the superconducting coherence length $\xi_0 = \hbar v/\Delta_0$ is small compared to the width of the junction W, the junction couples the co-propagating Majorana fermions χ_1 and χ_2 at values near $\varphi = \pi$. In Fig. I.3 the band structure of the junction is shown. The superconducting gap is $|\Delta| = 0.95\hbar v/a$ which results in an effective gap of $0.116\hbar v/a$. The time during which the injection takes place is [18]:

$$t_{\text{inj}} = \frac{\xi_0}{W}\left(\frac{\mathrm{d}\varphi}{\mathrm{d}t}\right)^{-1}.$$

In particular, if the Josephson phase is increased linearly from 0 to 2π over a duration τ, the injection time is $t_{\text{inj}} = \tau/\Delta_0 W$ in units where $\hbar = 1, v = 1$. One might be interested in an injection time that is shorter than the propagation time vL and shorter than the coherence time of hybridized edge states or states which participate in the excitation otherwise [28, 29]. In particular, the possible role of higher bound states of the junction in the injection can be investigated.

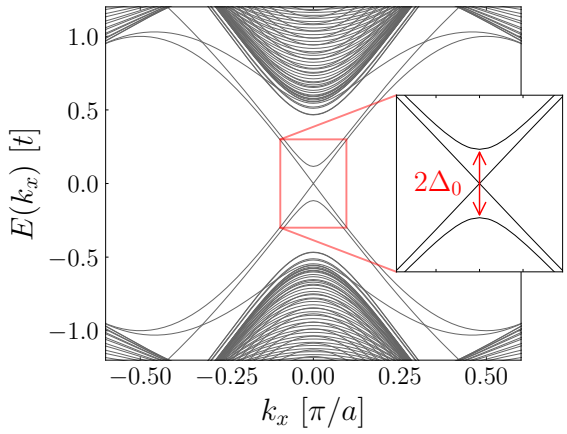

Figure I.3: Band structure of an infinitely long junction in the x direction for a system of 50 sites in the y direction, realized by a topological insulator of thickness 2 unit cells which separates two topological superconductors with no phase difference $\varphi = 0$. The chiral edge states in the junction couple, which opens an effective gap Δ_0. The gap closes with φ as $\Delta_0 \cos(\varphi/2)$.

■ Chapter II
Effective theory

This chapter briefly introduces the effective models obtained in Refs. [18, 22] as they will be used in our discussion as comparison. This also introduces the coupling ranges in the dynamical problem.

1. Scattering phase of the junction

Scattering of co-propagating Majorana edge states.— Following Ref. [18] (supplemental material), consider a point Josephson junction with a phase difference φ. If the amplitudes of incoming bottom and top Majorana edge states have respective amplitudes $\psi_{\text{in}} = (a_1, a_2)^\intercal$ (denoted χ_1 and χ_2 in Fig. I.2) then the outgoing amplitudes are:

$$\psi_{\text{out}} = \begin{pmatrix} b_1 \\ b_2 \end{pmatrix} = S_p(\varphi) \begin{pmatrix} a_1 \\ a_2 \end{pmatrix} \tag{2.1}$$

where $S_p(\varphi) = e^{i\varphi\sigma_y}$ is the scattering matrix. If the junction has width W then the scattering matrix is:

$$S_J = e^{i\alpha\sigma_y} \quad \text{with} \quad \alpha(\varphi) = \operatorname{sgn}(\varphi) \arccos\left(\frac{\cos(\varphi/2) + \tanh\beta}{1 + \cos(\varphi/2)\tanh\beta}\right)$$

where $\beta = W/\xi_0 \cos(\varphi/2)$ and $\xi_0 = \Delta_0/\hbar v$ the superconducting coherence length corresponding to the effective gap in the junction. $\alpha(\varphi)$ is the scattering phase. Thus the junction couples both edges for a select range of α near values of π, which we show in Fig. II.1 (left part). This range is given by the ratio W/ξ_0 and the ratio t_{inj}/τ must be equal to W/ξ_0 as well. These scattering phases were confirmed numerically in Ref. [18] as well.

Spatial model.— Following Ref. [22] consider two such junctions separated by a distance L. Then the effective Hamiltonian for the edge is:

$$H = iv \begin{pmatrix} -\partial_y & -h(y)\alpha(t) \\ h(y)\alpha(t) & -\partial_y \end{pmatrix} \tag{2.2}$$

where $h(y) = \delta(y) - \delta(y - L)$ are the positional terms for the infinitely thin junctions so that the Schrödinger equation $i\partial_t\psi = H\psi$ yields solutions of the form:

$$\psi(y,t) = \psi_0(y - vt)e^{i\sigma_y\Lambda(y,t)}$$

where $\Lambda(y,t)$ is the phase profile seen in Fig. I.2 and given by (in units of $v = 1$):

$$\Lambda(y,t) = (-1)^{N_{\text{vortex}}(L)}\alpha(t - y + L)\theta(y - L) - (-1)^{N_{\text{vortex}}(0)}\alpha(t - y)\theta(y)$$

where $\theta(y)$ denotes the Heaviside step function and $N_{\text{vortex}}(y_0)$ the number of vortices in the range $y > y_0$.

2. Charge quantization

The model [18] results in a perfect charge quantization due to a scattering phase difference which is exactly π: $S_J(2\pi) = S_J(0) + \pi$ independent of W/ξ_0. In the frozen scattering approximation (i.e. time dependence is only explicitely considered in $S(\varphi) = S(\varphi(t))$) the current at the exit of the superconductor produced by the braiding process be shown to be:

$$I(t) = j(t) + (-1)^{N_{\text{vortex}}} J(t - L/v) \quad \text{where} \quad J(t) := \frac{e}{2\pi}\partial_t \alpha(t) \tag{2.3}$$

which also holds when $L = 0$. Ref. [22] studied the case where the edge-vortices have a path-length difference δ which instead results in:

$$I_\delta(t) = J_\delta(t) + (-1)^{N_{\text{vortex}}} J_\delta(t-L) \quad \text{where} \quad J_\delta(t) := \frac{e}{2\pi}\frac{\sin(\alpha(t+\delta) - \alpha(t))}{\delta}. \tag{2.4}$$

Both approximations are shown in Fig. II.1 (right part) for $W/\xi_0 = 3, 8$ and assuming that the Josephson phase increases linearly from 0 to 2π over a duration τ. When integrated, the current pulse $Q(t) = \int_0^\tau \mathrm{d}t I(t)$ gives exactly $e/2$ or less if a path-length difference exists between the edge-vortices.

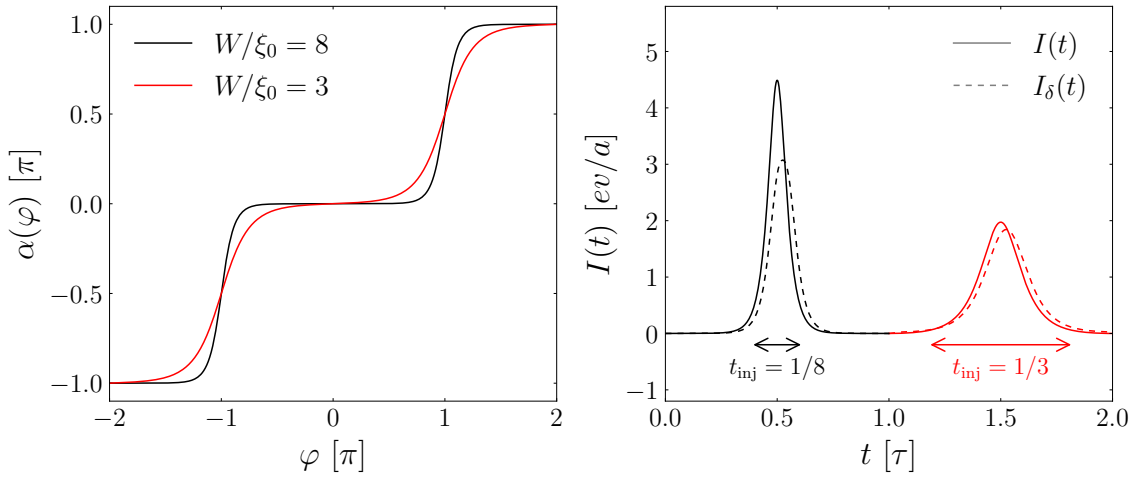

Figure II.1: (Left) Scattering phase $\alpha(\varphi)$ of two co-propagating Majorana fermions at a Josephson junction as a function of the Josephson phase φ, for two ratios W/ξ_0. The scattering phase is 4π periodic. (Right) Two current pulses corresponding to the ratios W/ξ_0 in the left plot. The injection time is given by $t_{\text{inj}} = \tau/(W/\xi_0)$. A dashed line shows the predicted current when a path-length difference δ (here $v\tau/20$) is induced. The unit of current density here assumes a distance unit a.

■ Chapter III
Continuum model

This chapter serves as an introduction to the Bogoliubov de Gennes theory. The Dirac Hamiltonian used to describe the edge fermions in the setup is introduced. The chapter ends with the continuum model for vortices and how they are integrated in the superconducting Hamiltonian while preserving gauge invariance.

1. Bogoliubov-de-Gennes approach

1.1. Mean-field superconductivity Hamiltonian

The mean-field Bardeen-Cooper-Schrieffer (BCS) Hamiltonian for superconductivity is given by [35]:

$$\hat{H} = \sum_{\mathbf{k},\sigma} (\varepsilon_{\mathbf{k}} - \mu)\ \hat{c}^{\dagger}_{\mathbf{k}\sigma}\hat{c}_{\mathbf{k}\sigma} + \sum_{\mathbf{k}} \Delta_{\mathbf{k}}\ \hat{c}^{\dagger}_{\mathbf{k}\uparrow}\hat{c}^{\dagger}_{-\mathbf{k}\downarrow} + \Delta^{*}_{\mathbf{k}}\ \hat{c}_{-\mathbf{k}\downarrow}\hat{c}_{\mathbf{k}\uparrow} \tag{3.1}$$

where $\hat{c}_{\mathbf{k}\sigma}$ ($\hat{c}^{\dagger}_{\mathbf{k}\sigma}$) is the annihilation (creation) operator of an electron with momentum $\mathbf{k}$ and spin $\sigma \in \{\uparrow, \downarrow\}$ acting on the Fock space. We refer to Ch.2-3. in Ref. [36] for an introduction to second quantization notation. Here, $\varepsilon_{\mathbf{k}}$ is a single electron dispersion, μ is the chemical potential and $\Delta_{\mathbf{k}}$ is the superconducting pairing potential which follows from the mean-field approximation. Note that the last two terms violate electron number conservation but not the electron number parity.

Background. Mean-field approximation.

The starting point is an effective Hamiltonian [37]

$$\hat{H} = \sum_{\mathbf{k},\sigma} (\varepsilon_{\mathbf{k}\sigma} - \mu)\hat{c}^{\dagger}_{\mathbf{k}\sigma}\hat{c}_{\mathbf{k}\sigma} + \frac{1}{N}\sum_{\mathbf{k},\mathbf{k}'} V_{\mathbf{k}\mathbf{k}'}(\hat{c}_{-\mathbf{k}\downarrow}\hat{c}_{\mathbf{k}\uparrow})^{\dagger}(\hat{c}_{-\mathbf{k}'\downarrow}\hat{c}_{\mathbf{k}'\uparrow})$$

where the left part is the usual electronic Hamiltonian and the right part now contains the creation of a Cooper pair at momentum $\mathbf{k}$ and annihilation at $\mathbf{k}'$ with an effective potential $V_{\mathbf{k}\mathbf{k}'}$. If one performs the mean field approximation:

$$\langle \hat{c}^{\dagger}_{\mathbf{k}\uparrow}\hat{c}^{\dagger}_{-\mathbf{k}\downarrow}\hat{c}_{-\mathbf{k}'\downarrow}\hat{c}_{\mathbf{k}'\uparrow}\rangle - \langle \hat{c}^{\dagger}_{\mathbf{k}\uparrow}\hat{c}^{\dagger}_{-\mathbf{k}\downarrow}\rangle \langle \hat{c}_{-\mathbf{k}'\downarrow}\hat{c}_{\mathbf{k}'\uparrow}\rangle \approx \langle \hat{c}^{\dagger}_{\mathbf{k}\uparrow}\hat{c}^{\dagger}_{-\mathbf{k}\downarrow}\rangle\, \hat{c}_{-\mathbf{k}'\downarrow}\hat{c}_{\mathbf{k}'\uparrow} + \hat{c}^{\dagger}_{\mathbf{k}\uparrow}\hat{c}^{\dagger}_{-\mathbf{k}\downarrow}\, \langle \hat{c}_{-\mathbf{k}'\downarrow}\hat{c}_{\mathbf{k}'\uparrow}\rangle$$

so that if we define $\Delta_{\mathbf{k}} = \frac{1}{N}\sum_{\mathbf{k}'} V_{\mathbf{k},\mathbf{k}'} \langle \hat{c}_{-\mathbf{k}'\downarrow}\hat{c}_{\mathbf{k}'\uparrow}\rangle$ the above Hamiltonian becomes:

$$\hat{H}_{\mathrm{MF}} = \sum_{\mathbf{k},\sigma} (\varepsilon_{\mathbf{k}\sigma} - \mu)\hat{c}^{\dagger}_{\mathbf{k}\sigma}\hat{c}_{\mathbf{k}\sigma} + \sum_{\mathbf{k}} \Delta_{\mathbf{k}}\ \hat{c}^{\dagger}_{\mathbf{k}\uparrow}\hat{c}^{\dagger}_{-\mathbf{k}\downarrow} + \Delta^{*}_{\mathbf{k}}\ \hat{c}_{-\mathbf{k}\downarrow}\hat{c}_{\mathbf{k}\uparrow} - \sum_{\mathbf{k}} \Delta_{\mathbf{k}}\, \langle \hat{c}^{\dagger}_{\mathbf{k}\uparrow}\hat{c}^{\dagger}_{-\mathbf{k}\downarrow}\rangle$$

1.2. Electron-hole doubling

It is possible to transform the above quadratic Hamiltonian into a single-particle Hamiltonian. One essentially makes a new artificial Hilbert space which has twice

the size of the single-electron Hilbert space. For this, all the terms above are written twice with a factor 1/2 in front and one uses the commutation relations:

$$\{\hat{c}^\dagger_{\mathbf{k}\sigma}, \hat{c}_{\mathbf{k}'\lambda}\} = \delta_{\mathbf{k}\mathbf{k}'}\delta_{\sigma\lambda} \quad \text{and} \quad \{\hat{c}_{\mathbf{k}\sigma}, \hat{c}_{\mathbf{k}'\lambda}\} = 0 \tag{3.2}$$

where δ denotes the Kronecker delta, to rewrite the Hamiltonian (3.1) as:

$$\begin{aligned}\hat{H} = &\sum_{\mathbf{k},\sigma} \frac{1}{2}(\varepsilon_{\mathbf{k}} - \mu)(\hat{c}^\dagger_{\mathbf{k}\sigma}\hat{c}_{\mathbf{k}\sigma} - \hat{c}_{\mathbf{k}\sigma}\hat{c}^\dagger_{\mathbf{k}\sigma} + 1) \\ &+ \sum_{\mathbf{k}} \frac{1}{2}\left(\Delta_{\mathbf{k}}\hat{c}^\dagger_{\mathbf{k}\uparrow}\hat{c}^\dagger_{-\mathbf{k}\downarrow} - \Delta_{-\mathbf{k}}\hat{c}^\dagger_{\mathbf{k}\downarrow}\hat{c}^\dagger_{-\mathbf{k}\uparrow}\right) + \frac{1}{2}(\Delta^*_{\mathbf{k}}\hat{c}_{-\mathbf{k}\downarrow}\hat{c}_{\mathbf{k}\uparrow} - \Delta^*_{-\mathbf{k}}\hat{c}_{-\mathbf{k}\uparrow}\hat{c}_{\mathbf{k}\downarrow}).\end{aligned}$$

Define the two component spinor containing the electron spins as $\hat{\mathbf{c}}_{\mathbf{k}} = (\hat{c}_{\mathbf{k}\uparrow}, \hat{c}_{\mathbf{k}\downarrow})^\intercal$ and the four component spinor $\hat{\Psi}_{\mathbf{k}} = (\hat{\mathbf{c}}_{\mathbf{k}}, \hat{\mathbf{c}}^\dagger_{-\mathbf{k}})^\intercal = ((\hat{c}_{\mathbf{k}\uparrow}, \hat{c}_{\mathbf{k}\downarrow}), (\hat{c}^\dagger_{-\mathbf{k}\uparrow}, \hat{c}^\dagger_{-\mathbf{k}\downarrow}))^\intercal$. Note that this is not a proper spinor as it takes electron creation and annihilation as two separate degrees of freedom. This redundancy is a central consideration here. For now electron annihilation in the bottom part of the spinor is thought of as the creation of a hole. Then the above can easily be rewritten as:

$$\hat{H} = \frac{1}{2}\sum_{\mathbf{k}} \hat{\Psi}^\dagger_{\mathbf{k}} h_{\mathrm{BdG}} \hat{\Psi}_{\mathbf{k}} + \sum_{\mathbf{k},\sigma} \varepsilon_{\mathbf{k}} \tag{3.3}$$

where we have defined the matrix:

$$h_{\mathrm{BdG}}(\mathbf{k}) = \begin{pmatrix} \varepsilon_{\mathbf{k}} - \mu & i\sigma_y\Delta_{\mathbf{k}} \\ -i\sigma_y\Delta^*_{\mathbf{k}} & \mu - \varepsilon_{-\mathbf{k}} \end{pmatrix}$$

where σ_y is one of the Pauli matrices. This is the Bogoliubov-de-Gennes (BdG) Hamiltonian matrix, where we assumed $\Delta_{\mathbf{k}} = \Delta_{-\mathbf{k}}$. This assumption corresponds with the case of singlet spin pairing [38]. So far we have done nothing but rewriting the mean-field Hamiltonian. The top left block is the single electron Hamiltonian, the bottom right block is the single hole Hamiltonian, and the other terms pair the electron and holes.

1.3. Bogoliubov quasiparticles

The above Hamiltonian can be diagonalized as a single-particle Hamiltonian. In fact, the diagonal form can be achieved by substituting the (unitary) Bogoliubov [39, 40] transformations:

$$\begin{pmatrix} \hat{c}_{\mathbf{k}\uparrow} \\ \hat{c}^\dagger_{-\mathbf{k}\downarrow} \end{pmatrix} = \begin{pmatrix} u^*_{\mathbf{k}} & v_{\mathbf{k}} \\ -v^*_{\mathbf{k}} & u_{\mathbf{k}} \end{pmatrix} \begin{pmatrix} \hat{d}_{\mathbf{k}\uparrow} \\ \hat{d}^\dagger_{-\mathbf{k}\downarrow} \end{pmatrix} \tag{3.4}$$

into equation (3.3) for some functions $u_{\mathbf{k}}, v_{\mathbf{k}}$ with $|u_{\mathbf{k}}|^2 + |v_{\mathbf{k}}|^2 = 1$. After some algebra to find the values of $u_{\mathbf{k}}, v_{\mathbf{k}}$ which diagonalise the equation (3.3) such that the new operators $\hat{d}_{\mathbf{k}\uparrow}, \hat{d}^\dagger_{-\mathbf{k}\downarrow}$ satisfy anti-commutation relations can be simplified into [38]:

$$\hat{H} = \sum_{\mathbf{k},\sigma} E_{\mathbf{k}} \hat{d}^\dagger_{\mathbf{k}\sigma}\hat{d}_{\mathbf{k}\sigma} + E_{\mathrm{GS}}$$

where $E_{\rm GS} := \sum_{\mathbf{k}} \varepsilon_{\mathbf{k}} - E_{\mathbf{k}}$ is the energy of the ground state up to a constant shift and $E_{\mathbf{k}}$ are the positive eigenvalues. The operators $\hat{d}_{\mathbf{k}\sigma}$ satisfy fermionic anti-commutation relations. Thus they are referred to as Bogoliubov quasiparticles. As seen above, they correspond with energy excitations of the ground state. Therefore, the latter is the vacuum state for the Bogoliubov quasiparticle operators:

$$\hat{d}_{\mathbf{k}\sigma} |\Omega\rangle = 0. \tag{3.5}$$

This is the starting point for reconstructing the wave-function of the well known BCS ground state $|\Omega\rangle$ [38]. A Hamiltonian which includes spin pairing leads to similar operators. We will treat these operators in more detail after discretizing momentum in Ch. IV.

1.4. Particle-hole symmetry

The Bogoliubov transformations can also be inverted:

$$\begin{pmatrix} \hat{d}_{\mathbf{k}\uparrow} \\ \hat{d}^\dagger_{-\mathbf{k}\downarrow} \end{pmatrix} = \begin{pmatrix} u_{\mathbf{k}} & -v_{\mathbf{k}} \\ v^*_{\mathbf{k}} & u^*_{\mathbf{k}} \end{pmatrix} \begin{pmatrix} \hat{c}_{\mathbf{k}\uparrow} \\ \hat{c}^\dagger_{-\mathbf{k}\downarrow} \end{pmatrix}.$$

The states $\hat{d}_{\mathbf{k}\uparrow}$ and $\hat{d}^\dagger_{-\mathbf{k}\downarrow}$ have opposite energy. They are respectively referred to as electron and hole excitations (because when $\Delta = 0$ they correspond to electrons and holes w.r.t. the Fermi level). They are related by particle-hole symmetry. Thus the particle-hole operator has to satisfy:

$$\mathcal{P} : \begin{pmatrix} u_{\mathbf{k}} & -v_{\mathbf{k}} \end{pmatrix}^\intercal \mapsto \begin{pmatrix} v^*_{\mathbf{k}} & u^*_{\mathbf{k}} \end{pmatrix}^\intercal$$

which is achieved by the operator $\mathcal{P} = -i\tau_y \mathcal{K}$. Here τ_y is the second Pauli matrix and $\mathcal{K}$ the operator of complex conjugation. The particle-hole operator is anti-unitary such that $\mathcal{P} i \mathcal{P}^{-1} = -i$.

2. Model of the topological insulator

We are interested in a platform which supports chiral Majorana fermions. Following the numerical model in Ref. [18], we adopt the Qi-Wu-Zhang Hamiltonian for a quantum anomalous Hall (QAH) insulator [34, 41] for a two-dimensional system. We first introduce the Hamiltonian, briefly describe its topological invariants, and derive its edge state spinors.

2.1. Hamiltonians

Topological insulator.— The electronic Hamiltonian for the QAH insulator is given by:

$$\hat{H}_{\rm QAH} = \sum_{\mathbf{k}} \hat{\mathbf{c}}^\dagger_{\mathbf{k}} h_e \hat{\mathbf{c}}_{\mathbf{k}} \tag{3.6}$$

where $\hat{\mathbf{c}}^\dagger_{\mathbf{k}} := (\hat{c}_{\mathbf{k}\uparrow}, \hat{c}_{\mathbf{k}\downarrow})^\intercal$ the spinors for electron spin as defined before, with [41]:

$$h_e(\mathbf{k}) = \begin{pmatrix} m(\mathbf{k}) & v(p_x - ip_y) \\ v(p_x + ip_y) & -m(\mathbf{k}) \end{pmatrix} = m(\mathbf{k})\sigma_z + v\mathbf{k} \cdot \boldsymbol{\sigma} \tag{3.7}$$

with $m(\mathbf{k}) = m_0\mathbf{k} + m_1\mathbf{k}^2$. Here, m_0 is a mass term, m_1 is a higher order mass term which will also be required to be nonzero in the real space discretization, and v is the velocity of the fermions. When $m_1 = 0$ this is the Dirac equation. On the right hand side we have abbreviated the matrix using the notation $\boldsymbol{\sigma} = (\sigma_x, \sigma_y)^\intercal$.

Topological superconductor.— When the QAH insulator is brought in proximity with a superconductor, it becomes a topological superconductor: it supports propagating states at its boundaries which are protected by the symmetries of the bulk, as we discuss in the next subsection. The superconducting Hamiltonian can be described in the BdG formalism analogous to equation (3.3) [34]:

$$\hat{H}_{\mathrm{BdG}} = \frac{1}{2}\sum_{\mathbf{k}} \hat{\Psi}^\dagger_{\mathbf{k}} h_e \hat{\Psi}_{\mathbf{k}} + \frac{1}{2}\operatorname{Tr} h_e \tag{3.8}$$

where again $\hat{\Psi} := (\hat{\mathbf{c}}_{\mathbf{k}}, \hat{\mathbf{c}}^\dagger_{-\mathbf{k}})^\intercal$ is the four component electron-hole spinor and:

$$h_{\mathrm{BdG}}(\mathbf{k}) = \begin{pmatrix} h_e(\mathbf{k}) - \mu & i\sigma_y\Delta_{\mathbf{k}} \\ -i\sigma_y\Delta^*_{\mathbf{k}} & \mu - h^*_e(-\mathbf{k}) \end{pmatrix}.$$

Basis change.— Another choice of basis is the one in which the electron-hole spinor is arranged differently as $\Psi_{\mathbf{k}} = ((\hat{c}_{\mathbf{k}\uparrow}, \hat{c}_{\mathbf{k}\downarrow}), (\hat{c}^\dagger_{-\mathbf{k}\downarrow}, -\hat{c}^\dagger_{-\mathbf{k}\uparrow}))^\intercal$ (Nambu representation) [42]. In this basis, the BdG Hamiltonian matrix has the more natural form:

$$h_{\mathrm{BdG}}(\mathbf{k}) = \begin{pmatrix} h_e(\mathbf{k}) & \Delta \\ \Delta^* & -\mathcal{T}h_e(\mathbf{k})\mathcal{T}^{-1} \end{pmatrix} = \begin{pmatrix} m(\mathbf{k})\sigma_z + v\mathbf{k}\cdot\boldsymbol{\sigma} & \Delta \\ \Delta^* & m(\mathbf{k})\sigma_z - v\mathbf{k}\cdot\boldsymbol{\sigma} \end{pmatrix} \tag{3.9}$$

where we set $\mu = 0$ as we will only consider zero Fermi energy in the future and have introduce the time reversal operator $\mathcal{T} = i\sigma_y\mathcal{K}$ and the pairing potential blocks are proportional to the identity matrix. Abbreviating Kronecker products by $\tau_i\sigma_j := \tau_i \otimes \sigma_j$ the particle-hole operator is now given by $\mathcal{P} = \tau_y\sigma_y\mathcal{K}$. We use this representation when discretizing the Hamiltonian in Ch. IV.

2.2. Topological phases

The topological invariant of the Hamiltonian (3.8) is the Chern number [34]:

$$\mathcal{N} = \frac{1}{2\pi}\sum_{E_n<0} \mathrm{d}k_x \mathrm{d}k_y \left(\partial_x a^n_y - \partial_y a^n_x\right)$$

with $a^n_j = \langle n\ \mathbf{k}| - i\partial_{k_j}|n\ \mathbf{k}\rangle$ the Berry phase connection in $\mathbf{k}$-space and n the band index. In the parameter range $m_0 > 0$ and $|\Delta| < |m_0|$, $\mathcal{N} = 0$ and the bulk is a trivial insulator (Ins). If $m_0 < 0$ and $|\Delta| < |m_0|$, then $\mathcal{N} = 2$ and the bulk is a topological insulator (TI). If $|\Delta| > |m_0|$ the region, $\mathcal{N} = 2$ and the bulk is a topological superconductor (TSC). This is summarized in the phase diagram Fig. III.1. The Chern number counts the number of edge states that exist at a domain wall between two regions in different phases: if $\mathcal{N} = \mathcal{N}_1$ for a region in space and $\mathcal{N} = \mathcal{N}_2$ for another region, then at their interface there exist $|\mathcal{N}_2 - \mathcal{N}_1|$ edge states. As shown in Fig. I.2 and Fig. III.1 the edge spinors which correspond to the co-propagating states in the edge-vortex setup are denoted by χ_1 and χ_2. Notice that when $\Delta > 0$ the spinor χ_1 corresponds with the TI/TSC interface while

for $\Delta < 0$ (i.e. $\varphi = \pi$ in $|\Delta|e^{i\varphi}$) it corresponds with the Ins/TSC interface as we show in the next subsection. Thus, if the superconducting gap is slowly inverted, the Majorana spinors are exchanged between the interfaces TI/TSC and Ins/TSC respectively, as shown in color between the edge-vortices in Fig. I.2. The edge-vortex can be pictured as the domain wall between these two fermionic spinors on a 1D boundary.

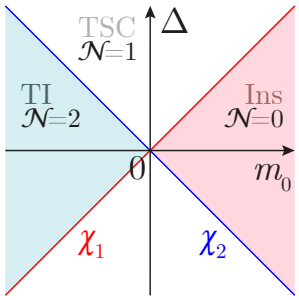

Figure III.1: Phase diagram of the QAH Hamiltonian with respective Chern numbes $\mathcal{N}$ for the topological insulator (TI), the trivial insulator (Ins) and the topological superconductor (TSC). The zero energy spinors at the boundaries are denoted χ_1 and χ_2 (blue and red lines). Diagram extended for $\Delta < 0$ based on Ref. [34]. The same color scheme as in the setup Fig. I.2 was used.

Toy model. The Kitaev chain.

The Kitaev chain [10] model illustrates well how a gap closing in the presence of particle-hole symmetry is related to the creation of unpaired Majorana zero-modes. We briefly summarize the introduction given by Ref. [43] where more details can be found. If one considers a superconducting Hamiltonian for a 1D chain of N spinless sites given by:

$$\hat{H}_{\mathrm{BdG}} = -\sum_{n=1}^{N} \mu\tau_z \, \hat{c}_n^\dagger \hat{c}_n - \sum_{n=1}^{N-1} (t\tau_z + i\Delta\tau_y) \, \hat{c}_n^\dagger \hat{c}_{n+1} + \mathrm{h.c.}$$

then, when the above Hamiltonian is expressed in terms of Majorana operators $\hat{c}_n^\dagger = \gamma_{2n-1} + i\gamma_{2n}$ (which is just a change of basis so far), the parameter range $\mu < 2t$ corresponds with the Majorana states being paired into their regular fermionic states as shown on the left:

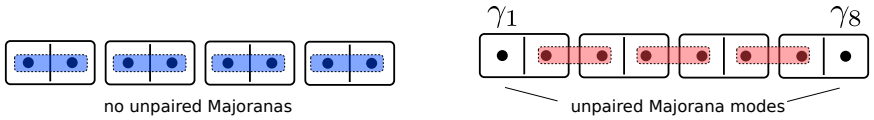

which is referred to as the trivial phase (images from [43]). However as soon as $\mu > 2t$ it becomes energetically favorable for Majoranas to pair with different neighbors, as shown in the right picture. This leaves two unpaired Majoranas at the edges: MZMs. These localized states are forced to stay there, otherwise violating particle-hole (PH) symmetry and are at $E = 0$. This is referred to as the topologically nontrivial phase. This same phenomenon can be described in a periodic Hamiltonian without boundaries. Then each bulk phase correspond with a different topological invariant $Q = \pm 1$ respectively (here related to the Pfaffian of the Hamiltonian) which does not change under continuous transformations of the Hamiltonian parameters within a phase. The only way to go from one topological invariant to another (a topological phase transition) i.e. the only way of bringing back / separating a pair of MZMs without breaking PH symmetry is to close the energy gap. At a spatial boundary between two regions with $Q = 1$ and $Q = -1$ respectively, an unpaired fermion must live at this domain wall (in the 1D case).

2.3. Matching edge-spinor solutions

Interface equation.— Here we solve for the spinors on the edges of the topological superconductor in the setup of Fig. I.2. We use these spinors as projectors in Ch. VI. Assuming Δ homogeneous and $m_1 = 0$, the Hamiltonian matrix (3.9) is:

$$h_{\rm BdG}(\mathbf{k}) = m_0\sigma_z + v\tau_z\mathbf{k}\cdot\boldsymbol{\sigma} + |\Delta|e^{-\varphi\tau_y}.$$

We adopt units of $\hbar = 1$ and $v = 1$. If k_y is a good quantum number and $k_x = -i\partial_x$ is dissolved in the spatial basis then the time-independent Schrödinger equation for zero energy solutions $h_{\rm BdG}\boldsymbol{\psi}(x) = 0$ can be simplified as:

$$\partial_x\boldsymbol{\psi}(x) = M\boldsymbol{\psi}(x) \tag{3.10}$$

where $M := -m_0\tau_z\sigma_y + k_y\sigma_z + \Delta(\cos\varphi\tau_y + \sin\varphi\tau_x)\sigma_x$.

Zero momentum solutions.— For $k_y = 0$ and $\varphi = 0$ so that $\Delta = \pm|\Delta|$, the eigenvectors and eigenvalues of M are respectively given by:

$$\begin{aligned}
\chi_1 &= 1/2\begin{pmatrix}-i & 1 & i & 1\end{pmatrix}^\intercal & \lambda_1 &= \Delta - m_0\\
\chi_2 &= 1/2\begin{pmatrix}i & -1 & i & 1\end{pmatrix}^\intercal & \lambda_2 &= -\Delta - m_0\\
\chi_3 &= 1/2\begin{pmatrix}i & 1 & -i & 1\end{pmatrix}^\intercal & \lambda_3 &= -\Delta + m_0\\
\chi_4 &= 1/2\begin{pmatrix}i & 1 & i & -1\end{pmatrix}^\intercal & \lambda_4 &= \Delta + m_0
\end{aligned}$$

with the general solution:

$$\psi(x) = \sum_{i=1}^{4} a_i\chi_i\exp(\lambda_i x), \qquad a_i \in \mathbb{C}.$$

Considering the three different interfaces Ins/TI, TI/TSC and TSC/Ins in Fig.I.2 (the first one of these interfaces is not shown there as it corresponds with the two counter propagating edge states) we can verify which of these basis states has a bounded solution at both sides of the interface. For example, assuming $\Delta > 0$, for the TSC/Ins interface $\Delta > |m_0|, m_0 < 0$ at the left – so the only growing solutions correspond to λ_1, λ_4 – and $\Delta = 0, m_0 > 0$ at the right – so the only decaying solutions correspond to λ_1, λ_2. Thus the only (unnormalized) basis solution allowed at that interface is, setting its location at $x = 0$, $\chi_1 f_1(x) := \chi_1[\exp((\Delta - m_0)x)\theta(-x) + \exp(-m_\infty x)\theta(x)]$ with $\theta(x)$ the Heaviside step function and $m_\infty > 0$ the mass term in the trivial insulator. Using a similar procedure we find that χ_2 is the only low energy spinor at the TI/TSC interface and χ_3, χ_4 are both located at the Ins/TI interface. Note that the localization lengths depend on the energy scales. In particular inside the TSC, χ_1 has a localization length $\hbar v/(\Delta + |m_0|)$ which is always smaller than the localization length $\hbar v/(\Delta - |m_0|)$ of χ_2 (since $m_0 < 0$ in the TSC). As we point out later, a large difference between these localization lengths induces path-length differences between the propagating edge-vortices. Finally, if $\Delta < 0$ the solution of the matching problem is such that χ_2 replaces χ_1 at the TSC/Ins interface, while the localization lengths are not affected by this. Finally, the edges correspond with the Bogoliubov operator (for $\pm k = 0$) $\gamma_1 = \int \mathrm{d}x f_1(x)\chi_1^\dagger\Psi_0$ for which – if we include a phase $e^{-i\pi/4}$ in χ_1 – it is easy to verify that $\gamma_1^\dagger = \gamma_1$. This is similar for the other spinors, showing that these edges indeed describe Majoranas. The above can be easily done for $k_y \neq 0$ to reconstruct the Majorana field on the edge (an effective edge description can be studied as in e.g. Refs. [29, 32, 34]).

Phase dependence.— The eigenvalues of M are real (it is Hermitian) and since $\varphi = 0, \pi$ yield opposite signs of Δ in the above eigenvalues, the eigenvalues cannot depend on φ in general. This is highly expected since φ is a gauge quantity (we study the case without vortices here). It is thus more general to include the phase in the spinors and now denote $\Delta = |\Delta|$ so that solving (3.10) yields:

$$\begin{aligned} \chi_1^\varphi &= 1/2 \begin{pmatrix} -ie^{i\varphi} & e^{i\varphi} & i & 1 \end{pmatrix}^\intercal \qquad & \lambda_1 &= \Delta - m_0 \\ \chi_2^\varphi &= 1/2 \begin{pmatrix} ie^{i\varphi} & -e^{i\varphi} & i & 1 \end{pmatrix}^\intercal \qquad & \lambda_2 &= -\Delta - m_0. \end{aligned}$$

The matching problem now always yields χ_1^φ at the TSC/Ins interface and χ_2^φ at the TI/TSC interface as opposed to the previous formulation. The geometric (Berry) phase on the edge of a translation invariant system under a change of $\varphi(t)$ can be calculated from these spinors which (for $j \in \{1, 2\}$) yields:

$$i \int_0^{\varphi(t)} \mathrm{d}\theta \; \chi_j^{\theta\dagger} \partial_\theta \chi_j^\phi = (-1)^j \frac{\varphi(t)}{2}$$

so the Majorana χ_2 on the top edge accumulates a phase $\varphi/2$ and χ_1 at the bottom edge a phase $-\varphi/2$, consistent with the theory (2.1).

3. Phase equations for superconducting vortices

In this section, we present the continuum equations for the phase which describes the vortices in the superconductor. We discuss the boundary conditions and include the vortices in the Hamiltonian.

3.1. Phase equations

Formulation in phase.— Let $\mathcal{C}$ be a simple closed contour in the superconductor (the latter described by $\Delta e^{i\phi}$ where $\phi : \Omega \to \mathbb{R}$ and $\Omega \subseteq \mathbb{R}^2$). Then the increment of the phase ϕ in the superconductor along the contour depends on the number of vortices inside the contour (see Background box below):

$$\oint_{\mathcal{C}} \nabla\phi \cdot \mathrm{d}\boldsymbol{\ell} = \iint_{\mathcal{S}} \nabla \times \nabla\phi \cdot \hat{z} \mathrm{d}S = 2\pi N_{\text{vortex}}^{\mathcal{S}} \tag{3.11a}$$

$$\nabla \cdot \nabla\phi = 0 \qquad \left(\text{or } \oint_{\mathcal{C}} \nabla\phi \cdot \mathbf{n} \; \mathrm{d}\ell = 0 \right) \tag{3.11b}$$

by Stokes' theorem and the divergence theorem, for *all* simply connected surfaces $\mathcal{S} \subseteq \Omega$ in the superconductor containing $N_{\text{vortex}}^{\mathcal{S}} \in \{0, 1, 2, ...\}$ vortices, where the unit vector $\hat{z}$ points upwards and the contour is counterclockwise. In the second line, we have included the continuity equation for the supercurrent, verified for all $\mathbf{r} \in \Omega$, so that the above set fully describes the phase in the superconductor. For the vortices, we will assume that their core is infinitely small i.e. for all $\mathcal{S}$ with $\iint_{\mathcal{S}} \nabla \times \nabla\phi \cdot \hat{z} \mathrm{d}S = 2\pi N$ there exists $\mathcal{S}' \subset \mathcal{S}$ such that this equality holds over $\mathcal{S}'$ too.

Formulation in supercurrent.— For a more natural treatment of boundary conditions, the above equations for the phase ϕ can be written in terms of the

supercurrent $\mathbf{j}(\mathbf{r})$ from (3.13). For simplicity let us define $\mathbf{v}(\mathbf{r}) := \mathbf{A} + \frac{1}{2}\nabla\phi \propto \mathbf{j}(\mathbf{r})$ in units of $\hbar = e = 1$. Then substitution results in analogous equations:

$$\iint_{\mathcal{S}} \nabla \times \mathbf{v}_s \cdot \hat{z}\mathrm{d}S = \pi(N^{\mathcal{S}}_{\text{vortex}} - N^{\Omega}_{\text{vortex}}) \tag{3.12a}$$

$$\nabla \cdot \mathbf{v}_s = 0 \tag{3.12b}$$

where we used $\nabla \times \mathbf{A} = \mathbf{B}$, the fact that the total flux is quantized with the number of vortices in Ω and the fact that $\oint_{\partial\Omega} \mathbf{j} \cdot \mathrm{d}\boldsymbol{\ell} = 0$. Here it is clearer that vortices are vorticity sources in the current field. For the magnetic field we will use the Landau gauge: $\mathbf{A} = B_0 x\hat{y}$ corresponding to $\mathbf{B} = B_0\hat{z} = -\pi N^{\Omega}_{\text{vortex}}\hat{z}/|\Omega|$ where $|\Omega|$ denotes the area of Ω.

Background. Vortices in superconductors.

Vortices are defects in type II superconductors where a magnetic field is allowed to locally penetrate and where superconductivity breaks down within a radius which corresponds with the penetration length. The supercurrent encircles a vortex. They were predicted to exist in the form of lattices by Abrikosov (Nobel prize 2003 [44]).

The supercurrent in the Ginzburg Landau theory is given by [45, 46]:

$$\mathbf{j}(\mathbf{r}) = -\frac{2e}{m^*}|\Delta|^2(2e\mathbf{A} + \hbar\nabla\phi) = -\frac{4e^2}{m^*}|\Delta|^2\left(\mathbf{A} + \frac{\Phi_0}{2\pi}\nabla\phi\right) \tag{3.13}$$

with $|\Delta|$ the ground state wave function, e the elementary charge, m^* the effective Cooper pair mass, $\mathbf{A}$ the vector potential, $\Phi_0 = 2\pi\hbar/e$ is the quantum of flux and ϕ the phase of the superconductor. Note that the gauge transformation which keeps this invariant is now $\mathbf{A} \to \mathbf{A}+\nabla f$ and $\phi \to \phi - 2\pi f/\Phi_0$ for a continuous function $f : \mathbb{R}^2 \to \mathbb{R}$.

Consider a hole with contour $\mathcal{C}$ in the superconductor pierced by a magnetic flux (a vortex, cf. picture below). Then the flux is quantized: taking the path integral of (3.13) along the entire boundary $\partial\Omega$ (which is zero) we get $\Phi_0 \oint_{\partial\Omega} \nabla\phi \cdot \mathrm{d}\boldsymbol{\ell} = \oint_{\partial\Omega} \mathbf{A} \cdot \mathrm{d}\boldsymbol{\ell} = 2\pi\Phi$. By singlevaluedness of the order parameter Δ, closed contours can only increase ϕ by 2π multiples so that $\int_{\mathcal{C}} \nabla\phi \cdot \mathrm{d}\boldsymbol{\ell} = 2\pi n$ for $n \in \mathbb{Z}$. Therefore, the flux caused by the magnetic field is quantized $\Phi = n\Phi_0$ in units of the magnetic flux quantum. Finally, if we require $\nabla \cdot \mathbf{j} = 0$ (stationary continuity equation with no sources) and assume the Coulomb gauge $\nabla \cdot \mathbf{A} = 0$ we obtain $\nabla \cdot \nabla\phi = 0$ as an extra condition on the phase.

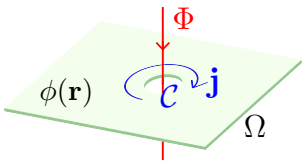

3.2. Boundary conditions

Closed (or Neumann).— For a closed system we require that no current goes through the boundary so that for any boundary vector $\mathbf{n}$ we have $\mathbf{v}_s \cdot \mathbf{n} = 0$. Assume that the domain $\Omega = (0, L_x) \times (0, L_y)$ is rectangular. Then the requirements on $\mathbf{v}_s$ are trivial in solving (3.11). Note that if one instead solves (3.12) the requirements

on $\nabla\phi$ are more complicated as they contain the vector potential terms:

$$\begin{cases} \partial_x\phi \mid_{\mathbf{r}=(0,y)} = 0 & \forall y \in (0, L_y) \\ \partial_x\phi \mid_{\mathbf{r}=(L_x,y)} = 0 & \forall y \in (0, L_y) \\ \partial_y\phi \mid_{\mathbf{r}=(x,0)} = 2B_0 x & \forall x \in (0, L_x) \\ \partial_y\phi \mid_{\mathbf{r}=(x,L_y)} = -2B_0 x & \forall x \in (0, L_x) \end{cases}. \tag{3.14}$$

Periodic.— Periodic boundary conditions for $\mathbf{v}_s$ in (3.12) are again trivial. To formulate boundary conditions in (3.11) first consider a periodic loop along the y direction i.e. $\mathbf{v}_s(x, 0) = \mathbf{v}_s(x, L_y)\ \forall x \in (0, L_x)$. Since $\mathbf{A}$ does not depend on y, the resulting condition on ϕ is also trivial: $\nabla\phi(x, 0) = \nabla\phi(x, L_y) = -2B_0 x\ \forall x \in (0, L_x)$. For a periodic loop in the x direction however, $\phi(x, y)$ cannot be periodic. Indeed, if we require that $\mathbf{v}_s(\mathbf{r})$ is periodic, then $\nabla\phi$ naturally has to compensate for the fact that $\mathbf{A} = B_0 x\hat{y}$ is not periodic. This problem can be corrected by using magnetic translations, which we introduce in the next subsection.

3.3. Hamiltonian description

Minimal coupling.— The newly introduced parameters are the phase ϕ of the vortices and the vector potential $\mathbf{A}$ (they together make up the only gauge invariant quantity associated with vortices which is the supercurrent $\mathbf{j}(\mathbf{r})$ as seen in (3.13)). Because we now introduce position dependent parameters in the momentum description, we treat $\phi, \mathbf{A}$ as operators so that $\phi = \phi(\hat{\mathbf{r}}), \mathbf{A} = \mathbf{A}(\hat{\mathbf{r}})$ where $\hat{\mathbf{r}}$ is the position operator. Then (3.8) becomes:

$$h_{\mathrm{BdG}}(\mathbf{k}) = \begin{pmatrix} h_e(\mathbf{k} + \mathbf{A}) & \Delta e^{i\phi} \\ \Delta^* e^{-i\phi} & -\mathcal{T} h_e(\mathbf{k} - \mathbf{A})\mathcal{T}^{-1} \end{pmatrix} \tag{3.15}$$

by minimal coupling. An extra homogeneous phase φ may still be allowed in Δ (later the Josephson phase).

Anderson gauge transformation.— Following Anderson [47] it is also possible to introduce the gauge transformation:

$$U_\phi = \begin{pmatrix} e^{i\phi} & 0 \\ 0 & 1 \end{pmatrix} \qquad \text{or} \qquad U_\phi = \begin{pmatrix} 1 & 0 \\ 0 & e^{-i\phi} \end{pmatrix}. \tag{3.16}$$

These are the only single valued transformations of that type for an arbitrary branch cut of ϕ. Applying the (left) gauge transformation on (3.9) gives:

$$h'_{\mathrm{BdG}}(\mathbf{k}) := U_\phi^{-1}\ h_{\mathrm{BdG}}(\mathbf{k})\ U_\phi = \begin{pmatrix} e^{-i\phi} h_e(\mathbf{k} + \mathbf{A}) e^{i\phi} & \Delta \\ \Delta^* & -\mathcal{T} h_e(\mathbf{k} - \mathbf{A})\mathcal{T}^{-1} \end{pmatrix}.$$

This transformation removed the phase of the vortices from the pairing potential, and moved it to the electron block of the Hamiltonian. It is easy to verify that the second Anderson transformation results in the phase being moved to the hole block. We now use the fact that for any operator $\hat{A}, \hat{B}$ such that $[\hat{A}, [\hat{A}, \hat{B}]] = 0$ we have $[f(\hat{A}), \hat{B}] = [\hat{A}, \hat{B}]\ \partial f(\hat{A})/\partial\hat{A}$. Furthermore the electron Hamiltonian can be expanded in $\mathbf{k}$ (this is the case explicitly in our Hamiltonian (3.7) and true in general). Then it follows that:

$$h_e(e^{-i\phi(\hat{\mathbf{r}})}\hat{\mathbf{k}}e^{i\phi(\hat{\mathbf{r}})}) = h_e([e^{-i\phi(\hat{\mathbf{r}})}, \hat{\mathbf{k}}]\ e^{i\phi(\hat{\mathbf{r}})} + \hat{\mathbf{k}}) = h_e([\hat{\mathbf{r}}, \hat{\mathbf{k}}](\nabla e^{-i\phi})e^{i\phi} + \hat{\mathbf{k}}) = h_e(\nabla\phi + \mathbf{k})$$

where we used the space-momentum commutator $[\hat{\mathbf{r}}, \hat{\mathbf{k}}] = i\mathbb{1}$ (with $\mathbb{1}$ a vector of ones). Thus we are left with a new Hamiltonian:

$$h'_{\mathrm{BdG}}(\mathbf{k}) = \begin{pmatrix} h_e(\mathbf{k} + \mathbf{A} + \nabla\phi) & \Delta \\ \Delta^* & -\mathcal{T}h_e(\mathbf{k} - \mathbf{A})\mathcal{T}^{-1} \end{pmatrix} \tag{3.17}$$

where, conveniently, knowledge of the gradient $\nabla\phi$ is sufficient to treat vortices. Furthermore, the branch-cut becomes irrelevant. However, this comes at the sacrifice of resolving the symmetry operators (particle-hole, charge conjugation, etc.) in a spatial basis.

Gauge invariant form.— It is worth noting that the $U(1)$ transformation for an electron $\hat{c}^\dagger_{\mathbf{k}} \to \hat{c}^\dagger_{\mathbf{k}} e^{i\theta}$ results in the following requirements:

$$\mathbf{A} \to \mathbf{A} + \nabla\theta \quad \text{and} \quad \phi \to \phi - 2\theta$$

to preserve the gauge invariance of the Hamiltonian, following a similar calculation as above. From this, it is immediately clear that the quantity $\mathbf{A} + \frac{1}{2}\nabla\phi$ is gauge invariant, which is consistent with our definition of $\mathbf{v}_s$. Then the only remaining gauge quantity in the Hamiltonian is $\mathbf{A}$:

$$h'_{\mathrm{BdG}}(\mathbf{k}) = \begin{pmatrix} h_e(\mathbf{k} - \mathbf{A} + 2\mathbf{v}_s) & \Delta \\ \Delta^* & -\mathcal{T}h_e(\mathbf{k} - \mathbf{A})\mathcal{T}^{-1} \end{pmatrix}. \tag{3.18}$$

■ Chapter IV
Discrete model

The BdG Hamiltonian is discretized in the tight-binding approximation. The phase equations for the vortices are also solved on a lattice as a result. Finally, the time-dependent problem is introduced. Spatial Bogoliubov operators are introduced in the stationary as well as the time-dependent cases. We conclude with the description of the ground state in the time-dependent problem.

1. Tight-binding discretization

1.1. General method

The basis transformation from momentum space to real space is given by the (inverse discrete Fourier) transform:

$$\hat{c}_k = \frac{1}{\sqrt{N}} \sum_{j=1}^{N} \hat{c}_j e^{-ikx_j}$$

where we assume a 1D system and no spin without loss of generality and $\hat{c}_j$ denotes the annihilation of a particle at site x_j. Suppose these discrete sites are separated by a lattice constant a so that $x_j = aj$ with $j \in \{1, ..., N\} := [N]$ (we will use this set notation in the future). To go to a spatial representation of our Hamiltonian (3.8) note that the Hamiltonian contains terms $\mathcal{O}(1), \mathcal{O}(k), \mathcal{O}(k^2)$. The basis transformation of a constant term is trivial and exact since:

$$\mathcal{O}(1) : \sum_k \hat{c}_k^\dagger \hat{c}_k = \frac{1}{N} \sum_{j,l=1}^{N} \hat{c}_j^\dagger \hat{c}_l \sum_k e^{ik(x_j - x_l)} = \frac{1}{N} \sum_{j,l=1}^{N} \hat{c}_j^\dagger \hat{c}_l N \delta_{jl} = \sum_{j=1}^{N} \hat{c}_j^\dagger \hat{c}_j$$

so the transformation of the terms such as μ and m_0 in real space is completely analogous to the terms in momentum. The real space transformation of the superconducting terms with Δ also results to analogous terms with the momentum space representation [48] provided Δ does not depend on $\mathbf{k}$. Now let us consider terms of higher order in k. First, recall that the discretness of real space implies a periodic momentum space as $e^{ikx_j} = e^{ikaj} = e^{i(ka+2\pi)j}$ so that values of $k \in [-\pi/a, \pi/a]$ are sufficient to describe the discretized Hamiltonian. The tight-binding approximation consists of approximating k by the periodic function $\sin(ka)/a$ and k^2 by $2(1-\cos(ka))/a^2$ which are the most natural periodic approximations in that interval for small k. To see why this corresponds with a real space discretization let us

expand the order k term similarly:

$$\begin{aligned}\mathcal{O}(k) : \sum_k k\ \hat{c}_k^\dagger \hat{c}_k &\approx \sum_k \frac{\sin(ka)}{a}\ \hat{c}_k^\dagger \hat{c}_k \\ &= \frac{1}{N}\sum_{j,l=1}^{N} \hat{c}_j^\dagger \hat{c}_l \sum_k \frac{1}{2ia}\left(e^{ika} - e^{-ika}\right) e^{ik(x_j - x_l)} \\ &= \frac{1}{2ia}\sum_{j,l=1}^{N} \hat{c}_j^\dagger \hat{c}_l (\delta_{j+1,l} - \delta_{j,l+1}) \\ &= \frac{1}{2ia}\sum_{j=1}^{N-1} \hat{c}_j^\dagger \hat{c}_{j+1} + \text{h.c.}\end{aligned}$$

where in the last step we have recognized the second term as the Hermitian conjugate of the first term. This term moves an electron from site j to site $j+1$ (and vice-versa) which is the well known real-space tight-binding Hamiltonian. In fact, this corresponds with the finite-difference approximation $\hat{k}\psi(x) = -i\partial_x\psi(x) \approx -i(\psi(x+a) - \psi(x-a))/(2a)$ of the momentum operator $\hat{k}$. For the term of order k^2 a similar procedure follows and results in:

$$\begin{aligned}\mathcal{O}(k^2) : \sum_k k^2\ \hat{c}_k^\dagger \hat{c}_k &\approx \sum_k \frac{2(1-\cos(ka))}{a^2}\ \hat{c}_k^\dagger \hat{c}_k \\ &= \frac{2}{a^2}\sum_{j=1}^{N} \hat{c}_j^\dagger \hat{c}_j - \frac{1}{a^2}\sum_{j=1}^{N-1} \hat{c}_j^\dagger \hat{c}_{j+1} + \text{h.c.}\end{aligned}$$

1.2. Tight-binding BdG Hamiltonian

We can now consider the direct space formulation of the BdG Hamiltonian (3.8). Let the Hilbert space consist of $2N$ electrons corresponding with N coordinates and 2 spins. Using a proper ordering of the spatial and spin coordinates we label $\hat{c}_{j\sigma}$ the electron annihilation operator of a spatial coordinate labeled j and spin σ. Then the second-quantized BdG Hamiltonian in real space is:

$$\hat{H}_{\text{BdG}} - \frac{1}{2}\operatorname{Tr} h_e = \frac{1}{2}\hat{\Psi}^\dagger \mathcal{H}_{\text{BdG}} \hat{\Psi} = \frac{1}{2}\sum_{i,j=1}^{N} \hat{\Psi}_i^\dagger \mathcal{H}_{\text{BdG}}(i,j)\hat{\Psi}_j \tag{4.1}$$

where $\mathcal{H}_{\text{BdG}}$ is the $4N \times 4N$ matrix which results after the momentum to space basis transformation, and $\hat{\Psi} := (\hat{\Psi}_1, ..., \hat{\Psi}_N)^\intercal$ is the $4N$-dimensional particle-hole spinor of the BdG theory with $\hat{\Psi}_j := (\hat{c}_{j\uparrow}, \hat{c}_{j\downarrow}, \hat{c}_{j\downarrow}^\dagger, -\hat{c}_{j\uparrow}^\dagger)^\intercal$ following the Nambu representation introduced in (3.9). After the tight-binding approximation for the real space formulation described in the previous subsection, it immediately follows that the matrix elements of $\mathcal{H}_{\text{BdG}}$ are (we only specify the upper diagonal part considering that $\mathcal{H}_{\text{BdG}}$ is Hermitian):

$$\mathcal{H}_{\text{BdG}}(i,j) = \begin{cases} h(i) & \forall i,j \text{ with } i = j, \\ t(i,j) & \forall i,j \text{ with } j = i+1, \\ 0 & \text{else,} \end{cases} \tag{4.2}$$

where the small 4×4 matrices are given by:

$$h(j) = (m_0 + 2m_1/a^2)\sigma_z + \Delta e^{i\tau_z \varphi} \tag{4.3}$$

$$t(j, j+1) = \frac{v}{2ia}\sigma_{x/y}\tau_z - \frac{m_1}{a^2}\sigma_z \tag{4.4}$$

for all $i, j \in [N]$ and where $\sigma_{x/y} = \sigma_x$ if $\mathbf{r}_{j+1} - \mathbf{r}_j = a\hat{x}$, $\sigma_{x/y} = \sigma_y$ if $\mathbf{r}_{j+1} - \mathbf{r}_j = a\hat{y}$, and $\sigma_{x/y} = 0$ else (there are no next-nearest neighbor terms). For the implementation of our tight-binding Hamiltonian we use the Kwant [49] library. Note that if our system consists of a domain with $100 \times 100 = 10^4$ sites, the Hamiltonian has dimensions $4N \times 4N = 4 \cdot 10^4 \times 4 \cdot 10^4$ so a non-sparse array would store $1.6 \cdot 10^9$ complex floats against at most $3 \cdot 4^2 \cdot N^2 = 4.8 \cdot 10^5$ for a sparse array. To treat closed boundary conditions the hopping elements t are simply defined as above for all interior sites $i \to i+1$ (and h.c.) for $i \in [N-1]$. To treat periodic boundary conditions, we provide the matrix with an additional condition "$t(N, 1)$" along the periodic direction, identical to (4.4).

1.3. Peierls substitution

The above discretization does not include vortices yet. We have ignored the presence of terms $\mathbf{A}$ and $\nabla\phi$ (or $\mathbf{v}_s$) obtained in equation (3.17) (or (3.18) respectively). The presence of these fields breaks the tight-binding approximation introduced before. Nevertheless they can instead be included via Peierls substitution in the Hamiltonian without vortices [50]:

$$\hat{c}_j^\dagger \hat{c}_l \to \hat{c}_j^\dagger \hat{c}_l \; e^{-i\int_{\mathbf{r}_l}^{\mathbf{r}_j} \mathbf{A}(\mathbf{r})\cdot \mathrm{d}\mathbf{r}} := \hat{c}_j^\dagger \hat{c}_l \; e^{-i\theta_{jl}}$$

where the integral goes over the shortest path from site j to site l. A number of demonstrations exist. To motivate this substitution with no ad-hoc argument consider an example where the field would be conservative: $\mathbf{A} = \nabla\theta$ for some $\theta(\mathbf{r})$. Then by the gradient theorem $\theta(\mathbf{r}) - \theta(\mathbf{0}) = \int_{\mathbf{0}}^{\mathbf{r}} \mathbf{A}(\mathbf{r}') \cdot \mathrm{d}\mathbf{r}'$ say over the shortest path from $\mathbf{0}$ to $\mathbf{r}$. Similar to the procedure used in simplifying the gauge transformation (3.16), we can write the problematic term $\mathbf{k} + \mathbf{A}(\hat{\mathbf{r}})$ (again, we adopt the operator form of $\mathbf{r}$ in the momentum basis) as $e^{-i(\theta(\hat{\mathbf{r}}) - \theta(\mathbf{0}))}\mathbf{k}e^{i(\theta(\hat{\mathbf{r}}) - \theta(\mathbf{0}))} = e^{-i\theta(\hat{\mathbf{r}})}\mathbf{k}e^{i\theta(\hat{\mathbf{r}})}$ instead. The Peierls substitution then naturally shows up in the tight-binding Hamiltonian:

$$\begin{aligned}
\sum_k \hat{c}_k^\dagger \; (k + A) \; \hat{c}_k &= \sum_k \hat{c}_k^\dagger \; (e^{-i\theta(\hat{x})} k e^{i\theta(\hat{x})}) \; \hat{c}_k \\
&\approx \frac{1}{N} \sum_{j,l=1}^{N} \sum_k e^{-i\theta(x_j)} \; \hat{c}_j^\dagger \frac{\sin(ka)}{a} \hat{c}_l \; e^{i\theta(x_l)} \\
&= \frac{1}{2ia} \sum_{j=1}^{N-1} \hat{c}_j^\dagger \hat{c}_{j+1} \; e^{-i\theta_{j+1,j}} + \text{h.c.}
\end{aligned}$$

where we went back to 1D for the sake of simplicity. Applying this substitution to other vector quantities results in the 4×4 hopping matrices from (4.4) modified. If we express everything in $\mathbf{A}$ and $\nabla\phi$ this becomes:

$$t(j, j+1) = \frac{v}{2ia}\sigma_{x/y} \begin{pmatrix} e^{-i\int_{\mathbf{r}_j}^{\mathbf{r}_{j+1}} (\mathbf{A} + \nabla\phi)\cdot \mathrm{d}\mathbf{r}} & 0 \\ 0 & -e^{i\int_{\mathbf{r}_j}^{\mathbf{r}_{j+1}} \mathbf{A}\cdot \mathrm{d}\mathbf{r}} \end{pmatrix} - \frac{m_1}{a^2}\sigma_z$$

for the Hamiltonian (3.17) and expressed in terms of $\mathbf{A}$ and $\mathbf{v}_s$ this becomes:

$$t(j,j+1) = \frac{v}{2ia}\sigma_{x/y}\begin{pmatrix} e^{i\int_{\mathrm{r}_j}^{\mathrm{r}_{j+1}}(\mathbf{A}-2\mathbf{v}_s)\cdot\mathrm{d}\mathbf{r}} & 0 \\ 0 & -e^{i\int_{\mathrm{r}_j}^{\mathrm{r}_{j+1}}\mathbf{A}\cdot\mathrm{d}\mathbf{r}} \end{pmatrix} - \frac{m_1}{a^2}\sigma_z$$

for the Hamiltonian (3.18).

2. Discretization of the superconducting phase

2.1. Discretized form

Both Peierls substitutions above are equivalent. Let us work with the first one so we solve the equation of the superconducting phase (3.11). Consider the phase $\phi : \Omega \to \mathbf{R}$ as before but now Ω a discrete domain identical to the one used in the tight-binding Hamiltonian. Let it have $N = n_x \times n_y$ sites, such that $(x_i, y_j) = ((i-1)a, (j-1)a)$ for $i \in [n_x]$ and $j \in [n_y]$. Then define:

$$\mathbf{s}(x_i, y_j) := \left(\int_{x_i}^{x_{i+1}} \mathrm{d}x\, \partial_x\phi\Big|_{y_j}, \int_{y_j}^{y_{j+1}} \mathrm{d}y\, \partial_y\phi\Big|_{x_j} \right)^{\mathsf{T}} := (s_x(i,j), s_y(i,j))^{\mathsf{T}} \tag{4.5}$$

for all $i \in [n_x - 1]$ and $j \in [n_y - 1]$, which correspond with the Peierls phase of vortices. If we define the oriented contour $\mathcal{C}_{ij}$ around a lattice cell $a \times a$ then the curl equation (3.11a) has to hold for *each* one of these contours. Similarly, evaluate the divergence integral (3.11b) over each closed contour. Thus, we simply evaluate (3.11a) and (3.11b) over each unit cell $\mathcal{C}_{ij}$ which results in the system:

$$\begin{cases} s_x(i,j) + s_y(i+1,j) - s_x(i,j+1) - s_y(i,j) = 2\pi N_{\mathrm{vortex}}^{\mathcal{S}_{ij}} \\ s_x(i,j) - s_x(i-1,j) + s_y(i,j) - s_y(i,j-1) = 0 \end{cases}$$

for all $i \in [n_x - 1], j \in [n_y - 1]$ and where $N_{\mathrm{vortex}}^{\mathcal{S}_{ij}}$ is the number of vortices inside the unit cell with index i, j. The contours are represented in Fig. IV.1. Note that, although the solutions are obtained on a discrete domain, they are exact.

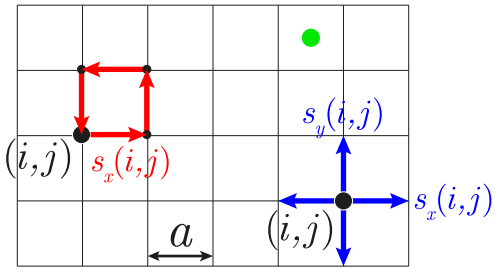

Figure IV.1: Vortex phase equations in terms of curl (red) and divergence (blue). The sum of the directed arrows gives the left hand side in the system of equations. The green dot represents a vortex, always in the middle of a unit cell.

2.2. Boundary conditions

To form a complete set, the above equations must be supplemented with boundary conditions. For periodic boundary conditions the curl equations above are used

again (with no vortices) but on the unit cell at the boundary (including opposite edges). This is similar for the divergence. For closed boundary conditions one imposes zero current through the boundary for which we refer to (3.14). For example at the boundary $x = n_x$ we require $s_x(n_x, j) = 0\ \forall j \in [n_y]$ in our gauge. For the boundary $y = n_y$ however, since the vector potential $\mathbf{A}$ is in the $\hat{y}$ direction the zero current condition is $s_y(i, n_y) = -2B_0 x_i\ \forall i \in [n_x]$. One should be careful though that the set is not overspecified. For example there are $2n_x n_y$ unknowns, the bulk equations solve $2(n_x - 1)(n_y - 1)$ but the periodic boundaries give $2(n_x + n_y) - 1$, so one equation must be removed.

2.3. Peierls phase integration

It is also possible not to perform the Anderson gauge transformation. Then, the Hamiltonian which includes the vortices is specified by (3.15): the phase $\phi(\mathbf{r})$ is a local quantity in the pairing potential and the vector potential enters the Hamiltonian by minimal coupling as usual. For this, we need to calculate $\phi(\mathbf{r})$. Naively one would sum up the integrals following the gradient theorem: $\phi(\mathbf{r}) - \phi(\mathbf{0}) = \int_{\mathbf{0}}^{\mathbf{r}} \nabla\phi(\mathbf{r}') \cdot \mathrm{d}\mathbf{r}'$ along any path. However $\nabla\phi$ is not conservative as it is path-dependent; a path which encircles the vortex will gain a phase of 2π and another path might avoid a vortex. Therefore, the choice of integration paths defines the location of the 2π jump. In Fig.IV.2 we show different paths associated with different phase accumulations. These simply correspond with different conventions applied consistently. Consider for example the left figure with $\phi(\mathbf{0}) = 0$ so that by telescoping:

$$\phi(x_i, y_j) = \sum_{k=1}^{i-1} s_x(k, 1) + \sum_{k=1}^{j-1} s_y(x_i, k).$$

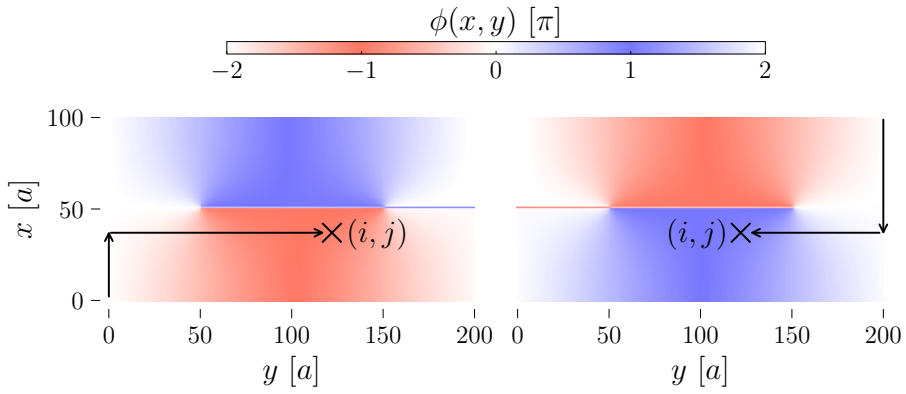

Figure IV.2: Different vortex 2π jumps as a function of the integration path.

3. Dynamical perturbation of the ground state

3.1. General time-dependent problem

So far we have considered a stationary problem governed by the time-independent Schrödinger equation. As introduced in Ch. I, the dynamical problem includes a homogeneous time-dependent Josephson phase $\varphi(t)$ in one of the superconducting regions. The latter is simply summed with the phase ϕ that describes the vortices

in the stationary Hamiltonian. Upon adding the dynamical phase $\varphi(t)$, the states are governed by the time-dependent Schrödinger equation:

$$i\partial_t \boldsymbol{\psi}(t) = \hat{H}_{\mathrm{BdG}}(t)\boldsymbol{\psi}(t), \qquad t > 0$$

where the initial condition $\boldsymbol{\psi}(0)$ is an arbitrary normalized vector of the $4N$-dimensional Hilbert space. The general solution of this time-dependent problem is given by:

$$\boldsymbol{\psi}(t) = \exp\left(-i\int_0^t \hat{H}_{\mathrm{BdG}}(s)\mathrm{d}s\right)\boldsymbol{\psi}(0) := \mathcal{U}(t)\boldsymbol{\psi}(0) \tag{4.6}$$

where we have defined the time-evolution operator $\mathcal{U}(t)$ (in matrix form corresponding with the above basis, or denoted $\hat{U}(t)$ in operator form) which is unitary.

3.2. Time evolution of Bogoliubov-de-Gennes states

Stationary quasiparticles.— In Ch. III equation (3.4) we have introduced the Bogolibuov quasiparticle operators in momentum space which diagonalize the BdG Hamiltonian. We now define them in direct space. Again, the tight-binding Hamiltonian BdG matrix (4.2) is diagonalized by the Bogoliubov transformation $\mathcal{V}$:

$$\mathcal{H}_{\mathrm{BdG}} = \mathcal{V}\mathcal{E}\mathcal{V}^*$$

with $\mathcal{E}$ the diagonal matrix containing the eigenvalues and $\mathcal{V}$ the eigenvectors of $\mathcal{H}_{\mathrm{BdG}}$ of the form:

$$\mathcal{V} = \begin{pmatrix} u & v^* \\ v & u^* \end{pmatrix} \tag{4.7}$$

where $u, v \in \mathbb{C}^{M\times M}$ where we define $M := 2N$. As a result, the eigenvalues come in positive/negative eigenvalue pairs which correspond to the particle/hole excitations respectively. It is simpler to introduce the following index notation:

Notation: Negative indices for negative eigenvalues.

Suppose the eigenvalues $\mathcal{E}_i$ are ordered along the diagonal of $\mathcal{E}$. Then define negative indices $-i$ with $i \in [M]$ or $i \in [-M]$ such that $E_{-i} := \mathcal{E}_{M-i}$ the negative eigenvalues, and redefine the positive indices as $E_i := \mathcal{E}_{M+i}$ the positive eigenvalues. Then $E_{-i} = -E_i \ \forall i \in [M]$. Define $\mathbb{Z}_M^* = [-M] \cup [M] = \{-M, ... -1\} \cup \{1, ..., M\}$.

The diagonalization may also be written in the operator form (4.1):

$$\hat{H}_{\mathrm{BdG}} - \frac{1}{2}\operatorname{Tr} h_e = \frac{1}{2}\hat{\Psi}^\dagger \mathcal{V}\mathcal{E}\mathcal{V}^*\hat{\Psi} = \frac{1}{2}\hat{\mathbf{d}}^\dagger \mathcal{E}\hat{\mathbf{d}}. \tag{4.8}$$

where we defined $\hat{\mathbf{d}} := \mathcal{V}^*\hat{\Psi}$. Note that by unitarity, $\hat{\Psi} = \mathcal{V}\hat{\mathbf{d}}$. The individual stationary Bogoliubov creation operators are then given by the elements of $\hat{\mathbf{d}}$ which can be expanded[1]:

$$\hat{d}_\alpha^\dagger = \sum_{j=1}^{M} u_{\alpha j}\hat{c}_j^\dagger + v_{\alpha j}\hat{c}_j \quad \text{and} \quad \hat{d}_\alpha = \sum_{j=1}^{M} u_{\alpha j}^*\hat{c}_j + v_{\alpha j}^*\hat{c}_j^\dagger \ \forall \alpha \in [M]. \tag{4.9}$$

[1]Because of the redundancy $\hat{d}_\alpha = \hat{d}_{-\alpha}^\dagger \ \forall \alpha \in [M]$, anti-commutation cannot hold across the whole spectrum: $\{\hat{d}_\alpha, \hat{d}_\beta\} = \{\hat{d}_{-\alpha}^\dagger, \hat{d}_\beta\} = \delta_{-\alpha,\beta} \neq 0$ if $\alpha = -\beta$. We can extend the anti-commutations to the whole spectrum to account for this: $\{\hat{d}_\alpha^\dagger, \hat{d}_\beta\} = \delta_{\alpha\beta}$ and $\{\hat{d}_\alpha, \hat{d}_\beta\} = \delta_{\alpha,-\beta} \ \forall \alpha, \beta \in \mathbb{Z}_N^*$.

Note that we have chosen α only positive. We have discarded all negative energy states because they are redundant. It is straightforward to show that the Bogoliubov operators again satisfy fermionic anti-commutation relations:

$$\{\hat{d}^\dagger_\alpha, \hat{d}_\beta\} = \delta_{\alpha\beta} \quad \text{and} \quad \{\hat{d}_\alpha, \hat{d}_\beta\} = 0 \quad \forall\alpha, \beta \in [M].$$

Time-evolved quasiparticles.— Note that the columns of $\mathcal{V}$ are orthonormal and that the evolution operator (4.6) is unitary so preserves the orthonormality. It can be easily shown [51] that the time-dependent operators:

$$\hat{a}^\dagger_\alpha := \hat{U}(t)\hat{d}^\dagger_\alpha\hat{U}^\dagger(t) \tag{4.10}$$

satisfy equal-time anti-commutation relations:

$$\{\hat{a}^\dagger_\alpha, \hat{a}_\beta\} = \delta_{\alpha\beta} \quad \text{and} \quad \{\hat{a}_\alpha, \hat{a}_\beta\} = 0 \quad \forall\alpha, \beta \in [M]$$

where the restriction to only positive indices is less evident but still true. Most importantly each one obeys the time-dependent Schrödinger equation $i\partial_t\psi_\alpha(t) = \mathcal{H}_{\text{BdG}}(t)\psi_\alpha(t)$ with $\psi_\alpha(t) = (u_{\alpha,-M}(t), ..., u_{\alpha,-1}(t), v_{\alpha,1}(t), ..., v_{\alpha,M}(t))^\intercal$ the coefficients in $\hat{a}^\dagger(t)$. Therefore, the full many-body evolution (4.6) requires solving the single-particle Schrödinger equation M times.

3.3. Construction of the ground state

As introduced in Ch. III equation (3.5) in momentum space, the stationary ground state is the vacuum state of the positive energy Bogoliubov quasiparticles:

$$\hat{d}_\alpha |\Omega\rangle = 0, \ \forall\alpha \in [M] \qquad \text{or} \qquad \hat{d}^\dagger_\alpha |\Omega\rangle = 0, \ \forall\alpha \in [-M] \tag{4.11}$$

where $|\Omega\rangle$ denotes the ground state of the Hamiltonian at $t = 0$, which is the initial state of the evolution. In Ch. V we will see that the complete knowledge of single-particle expectation values in the evolved state is provided by the evolved negative energy eigenstates, without explicitly knowing the wave function of $|\Omega\rangle$. Nevertheless in Ch. VII it will be useful to introduce another vacuum state $|\text{vac}\rangle$ which satisfies:

$$\hat{d}_\alpha |\text{vac}\rangle = 0, \ \forall\alpha \in [-M] \qquad \text{or} \qquad \hat{d}^\dagger_\alpha |\text{vac}\rangle = 0, \ \forall\alpha \in [M] \tag{4.12}$$

which is the exact opposite of (4.11). This allows us to write the ground state as:

$$|\Omega\rangle = \prod_{\alpha\in[-M]} \hat{d}^\dagger_\alpha |\text{vac}\rangle \,. \tag{4.13}$$

We will refer to this description as the Fermi picture since it corresponds with filling a vacuum with negative energy excitations. Then, the evolved state has the more intuitive form:

$$\hat{U}(t)|\Omega\rangle = \hat{U}(t)\prod_{\alpha\in[-M]} \hat{d}^\dagger_\alpha |\text{vac}\rangle = \left(\prod_{\alpha\in[-M]} a^\dagger_\alpha(t)\right)\hat{U}(t)|\text{vac}\rangle \tag{4.14}$$

which follows by inserting identities $\hat{U}^\dagger\hat{U}$ in the product and using the definition (4.10), so that this is a product of (mutually anti-commuting) time-evolved quasi-particles. The definition of $|\text{vac}\rangle$ is unusual however as it consists of the state which is completely filled with the positive energy excitations. However it can be used to describe e.g. transitions more intuitively while remaining entirely correct [52].

3.4. Numerical time-evolution scheme

The time evolution is done using the library Tkwant [53] and each single-particle evolution is done in parallel, consisting of typically between 30 and 100 single-particle evolutions per simulation, done on nodes of each 9.6 TFLOPS. Tkwant uses the Dormand-Prince 5(4) Runge-Kutta variation [54] provided by the SciPy library. The relative tolerance is set at 10^{-9}.

■ Chapter V
Operators in the evolved ground state

This chapter treats the evaluation of single-particle observables in the evolved ground state. This is a many-body problem which requires a careful treatment of the BdG redundancy. The necessary operator decompositions are introduced first, and applied to the evolved ground state in the second part.

1. Stationary expectation values

1.1. Spectral decompositions

In the standard electron basis.— Let $\hat{Q}$ be an arbitrary single-electron Hermitian operator (such as charge or current density). Then it can be dissolved in the electronic basis:

$$\hat{Q} = \sum_{i,j=1}^{N} \mathcal{Q}^e_{ij} \hat{c_i}^\dagger \hat{c}_j \tag{5.1}$$

where $\mathcal{Q}^e_{ij}$ is the matrix element $\langle i|\hat{Q}|j\rangle$ of the operator known for electrons. For the operator of charge, this is just the constant elementary charge $\mathcal{Q}^e_{ij} = e \cdot \delta_{ij}$. Note that the sum goes until N; we neglect spin in this chapter because we only discuss the particle-hole part here.

In the redundant electron-hole basis.— We can apply the same method as when we introduced the BdG Hamiltonian in Ch.III to write the above operator $\hat{Q}$ in the particle-hole basis by using anti-commutation relations:

$$\begin{aligned}
\hat{Q} &= \sum_{i,j=1}^{N} \mathcal{Q}^e_{ij} \frac{1}{2}(\hat{c_i}^\dagger \hat{c}_j + \delta_{ij} - \hat{c}_j \hat{c_i}^\dagger) \\
&= \sum_{i,j=1}^{N} \frac{1}{2} \begin{pmatrix} \hat{c}_i^\dagger \end{pmatrix}^\intercal \begin{pmatrix} \mathcal{Q}^e_{ij} & 0 \\ 0 & -\mathcal{Q}^e_{ji} \end{pmatrix} \begin{pmatrix} \hat{c}_j \\ \hat{c}_j^\dagger \end{pmatrix} + \frac{1}{2} \operatorname{Tr} \mathcal{Q}_e \\
&= \sum_{i,j=1}^{N} \frac{1}{2} \hat{\Psi}_i^\dagger \mathcal{Q}^{\mathrm{BdG}}_{ij} \hat{\Psi}_j + \frac{1}{2} \operatorname{Tr} \mathcal{Q}_e \\
\hat{Q} &= \frac{1}{2} \hat{\Psi}^\dagger \mathcal{Q}_{\mathrm{BdG}} \hat{\Psi} + \frac{1}{2} \operatorname{Tr} \mathcal{Q}_e
\end{aligned} \tag{5.2}$$

where the spinors are $\hat{\Psi} = (\hat{\Psi}_1, ..., \hat{\Psi}_2)^\intercal$.

In the redundant quasi-particle basis.— The expression above allows us to substitute the Bogoliubov transformations (4.9) $\hat{\Psi} = \mathcal{V}\hat{\mathbf{d}}$:

$$\hat{Q} - \frac{1}{2} \operatorname{Tr} \mathcal{Q}_e = \frac{1}{2} \hat{\mathbf{d}}^\dagger (\mathcal{V}^* \mathcal{Q}_{\mathrm{BdG}} \mathcal{V}) \hat{\mathbf{d}} := \frac{1}{2} \hat{\mathbf{d}}^\dagger \widetilde{\mathcal{Q}} \hat{\mathbf{d}} \tag{5.3}$$

where we have brought the constant trace to the left. This can also be expanded as:

$$\hat{Q} - \frac{1}{2}\operatorname{Tr}\mathcal{Q}_e = \frac{1}{2}\sum_{\alpha,\beta=1}^{2N} \widetilde{\mathcal{Q}}_{\alpha\beta}\hat{d}^\dagger_\alpha \hat{d}_\beta.$$

If we denote the columns of $\mathcal{V}$ (i.e. the eigenvectors of $\mathcal{H}_{\mathrm{BdG}}$) by $\boldsymbol{\psi}_\alpha = (u_\alpha, v_\alpha)^\intercal$ (for $\alpha \in [N]$) with eigenvalue E_α then the matrix elements of $\widetilde{\mathcal{Q}}$ can be written more intuitively as $\boldsymbol{\psi}^*_\alpha \mathcal{Q}_{\mathrm{BdG}} \boldsymbol{\psi}_\beta$ (a common inner product through $\mathcal{Q}_{\mathrm{BdG}}$).

In a non-redundant quasi-particle basis.— The above decomposition involves quasi-particle creation operators which do not mutually anti-commute. We remove this redundancy by expressing the above in only positive indices $\alpha, \beta \in [N]$. For this note the particle-hole symmetry of the twiddled charge:

$$\widetilde{\mathcal{Q}} = \begin{pmatrix} \widetilde{\mathcal{Q}}_{++} & \widetilde{\mathcal{Q}}_{+-} \\ \widetilde{\mathcal{Q}}_{-+} & \widetilde{\mathcal{Q}}_{--} \end{pmatrix} = \begin{pmatrix} \widetilde{\mathcal{Q}}_{++} & \widetilde{\mathcal{Q}}_{+-} \\ \widetilde{\mathcal{Q}}^*_{+-} & -\widetilde{\mathcal{Q}}^\intercal_{++} \end{pmatrix}$$

The above can be shown by substituting the Bogoliubov transformation $\mathcal{V}$ (4.7) in the definition of $\widetilde{\mathcal{Q}} = \mathcal{V}^* \mathcal{Q}_{\mathrm{BdG}} \mathcal{V}$. Expanding the blocks of the $\widetilde{\mathcal{Q}}$ matrix in the operator and simplifying using anti-commutation relations yields:

$$\hat{Q} - \frac{1}{2}\operatorname{Tr}\mathcal{Q}_e = \sum_{\alpha,\beta=1}^{N} \widetilde{\mathcal{Q}}^{++}_{\alpha\beta}\hat{d}^\dagger_\alpha \hat{d}_\beta - \frac{1}{2}\operatorname{Tr}\Big\{\widetilde{\mathcal{Q}}_{++}\Big\} + \frac{1}{2}\left(\sum_{\alpha,\beta=1}^{N} \widetilde{\mathcal{Q}}^{+-}_{\alpha\beta}\hat{d}^\dagger_\alpha \hat{d}^\dagger_\beta + \text{h.c.}\right) \tag{5.4}$$

which is reminiscent of the quadratic BdG Hamiltonian in its original form (3.1).

1.2. Ground state expectation value

If we now consider the stationary ground state $|\Omega\rangle$ one immediately gets:

$$\begin{aligned} \langle \hat{Q} \rangle &= \langle \Omega | \hat{Q} | \Omega \rangle \\ &= \frac{1}{2}\operatorname{Tr}\mathcal{Q}_e - \frac{1}{2}\operatorname{Tr}\Big\{\widetilde{\mathcal{Q}}_{++}\Big\} \end{aligned}$$

from the above (5.4), since it is annihilated by the leftmost and rightmost terms by construction of the vacuum. For example, for the total charge in the system this is $Ne/2 - \sum_{\alpha=1}^{N} \boldsymbol{\psi}^*_\alpha \mathcal{Q}_{\mathrm{BdG}} \boldsymbol{\psi}_\alpha / 2$ the sum over each excitation's charge expectation.

2. Dynamical expectation values

We now consider observables $\langle Q \rangle(t) = \langle \Omega | \hat{U}^\dagger \hat{Q} \hat{U} | \Omega \rangle$ in the time-evolved ground state. Because we treat operators in the Heisenberg picture it is convenient to introduce the operator $\hat{\mathbf{d}}(t) = \hat{U}^\dagger(t)\hat{\mathbf{d}}\hat{U}(t)$. Note that this is different from $\hat{\mathbf{a}}(t)$ (4.10) by the fact that the unitary operator is now on the right of the creation operator. This is still simply a rotation of the basis – which preserves anti-commutation relations – which we write:

$$\hat{d}_\alpha(t) = \sum_{\beta \in \mathbb{Z}^*_N} \mathcal{R}_{\alpha\beta}(t)\hat{d}_\beta \quad \text{or} \quad \hat{\mathbf{d}}(t) = \mathcal{R}(t)\hat{\mathbf{d}}. \tag{5.5}$$

The latter transformation is related to the time evolution operator by conjugate-transposition i.e. its elements $\alpha\beta$ are given by the inner products $\langle \boldsymbol{\psi}_\alpha(0), \boldsymbol{\psi}_\beta(t)\rangle$ which we denote $\langle \boldsymbol{\psi}^0_\alpha, \boldsymbol{\psi}^t_\beta\rangle$ for simplicity. After some algebra it is possible to show that:

$$\mathcal{R} = \mathcal{V}^*\mathcal{V}(t)\mathcal{V} \tag{5.6}$$

where $\mathcal{V}(t)$ is the matrix whose columns α satisfy the time-dependent Schrödinger equations.

2.1. In the electron-hole basis

Consider the time-dependent equivalent of the completeness relation (5.3) by applying $\hat{U}$ on both sides and inserting identities:

$$\begin{aligned}
\hat{U}^\dagger\hat{Q}\hat{U} - \frac{1}{2}\operatorname{Tr}\mathcal{Q}_e &= \frac{1}{2}\hat{U}^\dagger\hat{\mathbf{d}}^\dagger(\mathcal{V}^*\mathcal{Q}_{\mathrm{BdG}}\mathcal{V})\hat{\mathbf{d}}\hat{U} \\
&= \frac{1}{2}\hat{U}^\dagger\hat{\mathbf{d}}^\dagger(\hat{U}\hat{U}^\dagger)(\mathcal{V}^*\mathcal{Q}_{\mathrm{BdG}}\mathcal{V})(\hat{U}\hat{U}^\dagger)\hat{\mathbf{d}}\hat{U} \\
&= \frac{1}{2}\hat{\mathbf{d}}^\dagger(\mathcal{R}^*(t)\mathcal{V}^*\mathcal{Q}_{\mathrm{BdG}}\mathcal{V}\mathcal{R}(t))\hat{\mathbf{d}} \\
&= \frac{1}{2}\hat{\mathbf{d}}^\dagger(\mathcal{V}^*\mathcal{V}^*(t)\mathcal{Q}_{\mathrm{BdG}}\mathcal{V}(t)\mathcal{V})\hat{\mathbf{d}}
\end{aligned}$$

One readily sees that the only terms which do not annihilate the vacuum are the ones with negative eigenvalues. Furthermore, the columns α of $\mathcal{V}(t)\mathcal{V}$ are the time-dependent solutions $\boldsymbol{\psi}_\alpha(t)$. Thus, the dynamical expectation of $\hat{Q}$ may be written:

$$\langle\hat{Q}(t)\rangle - \frac{1}{2}\operatorname{Tr}\mathcal{Q}_e = \langle\Omega|\hat{U}^\dagger\hat{Q}\hat{U}|\Omega\rangle = \frac{1}{2}\sum_{\alpha\in[-N]}\boldsymbol{\psi}^{*t}_\alpha\mathcal{Q}_{\mathrm{BdG}}\boldsymbol{\psi}^t_\alpha$$

so that the net change over time – written in a first quantized notation – is:

$$\langle\hat{Q}(t)\rangle - \langle\hat{Q}(0)\rangle = \frac{1}{2}\sum_{\alpha\in[-N]}\langle\alpha^t|\hat{Q}|\alpha^t\rangle - \langle\alpha^0|\hat{Q}|\alpha^0\rangle\,. \tag{5.7}$$

This expression is intuitive as it is completely analogous to the expectation value in conventional (semi-)conductors, where the expectation value is the sum over all single-particle expectations below the Fermi surface $E = 0$. In the case of the redundant BdG theory however, this result is not trivial. We will see that if one introduces a cut-off in the index $\alpha \in [-N_{\mathrm{cutoff}}]$ with $N_{\mathrm{cutoff}} < N$ – which is usually a cut-off in energies far from the Fermi surface – this sum does not converge for increasing values of N_{cutoff}. We propose an alternative in the next subsection.

2.2. In the stationary basis

Consider the stationary spectral decomposition (5.4) applied to the evolved vacuum. This results in the expression:

$$\begin{aligned}
\hat{U}^\dagger\hat{Q}\hat{U} - \frac{1}{2}\operatorname{Tr}\mathcal{Q}_e + \frac{1}{2}\operatorname{Tr}\Big\{\widetilde{\mathcal{Q}}_{++}\Big\} &= \sum_{\alpha,\beta=1}^{N}\widetilde{\mathcal{Q}}^{++}_{\alpha\beta}\hat{U}^\dagger\hat{d}^\dagger_\alpha\hat{d}_\beta\hat{U} + \frac{1}{2}\left(\sum_{\alpha,\beta=1}^{N}\widetilde{\mathcal{Q}}^{+-}_{\alpha\beta}\hat{U}^\dagger\hat{d}^\dagger_\alpha\hat{d}^\dagger_\beta\hat{U} + \text{h.c.}\right) \\
&:= \hat{A}(t) + \frac{1}{2}(\hat{B}(t) + \text{h.c.})
\end{aligned}$$

where we have labeled the terms $\hat{A}$ and $\hat{B}$. We develop individual terms by substituting (5.5) and split the sums in four energy sectors (analogous to in (5.4)):

$$\begin{aligned}\hat{U}^\dagger \hat{d}^\dagger_\alpha \hat{d}_\beta \hat{U} &= \sum_{i,j\in\mathbb{Z}^*_N} \mathcal{R}^*_{\alpha i}\mathcal{R}_{\beta j}\hat{d}^\dagger_i \hat{d}_j \\ &= \left(\sum_{i,j\in[N]} + \sum_{i,j\in[\pm N]} + \sum_{i,j\in[\mp N]} + \sum_{i,j\in[-N]}\right)(\mathcal{R}^*_{\alpha i}\mathcal{R}_{\beta j}\hat{d}^\dagger_i \hat{d}_j). \end{aligned} \tag{5.8}$$

Clearly, the only nonzero contribution in the vacuum is the last term over negative indices, which yields $\langle\Omega|\hat{d}^\dagger_i\hat{d}_j|\Omega\rangle = \delta_{ij}$ so that:

$$\begin{aligned}\langle\Omega|\hat{A}(t)|\Omega\rangle &= \sum_{\alpha,\beta\in[N]} \widetilde{\mathcal{Q}}^{++}_{\alpha\beta} \sum_{\gamma\in[N]} \mathcal{R}^*_{\alpha-\gamma}\mathcal{R}_{\beta-\gamma} \\ &= \sum_{\alpha,\beta,\gamma\in[N]} \widetilde{\mathcal{Q}}^{++}_{\alpha\beta}\ \langle \boldsymbol{\psi}^t_{-\gamma}, \boldsymbol{\psi}^0_\alpha\rangle \langle \boldsymbol{\psi}^0_\beta, \boldsymbol{\psi}^t_{-\gamma}\rangle\,. \end{aligned}$$

Note that the only terms which contribute here are the evolved states that are *below* $E = 0$ at $t = 0$. Therefore, we only need to evolve negative energy eigenstates which is consistent with (5.7). For the case of charge in our system this will be the main contribution. Let us now consider the second order term $\hat{B}(t)$ and its Hermitian conjugate. Again substituting (5.5) and splitting in energy sectors as in (5.8) only allows for terms of the form $\langle\hat{d}^\dagger_i\hat{d}^\dagger_j\rangle$ with $i \in [-N]$ and $j \in [N]$ to be nonzero, which yields δ_{ij} and thus:

$$\begin{aligned}\langle\Omega|\hat{B}(t)|\Omega\rangle &= \sum_{\alpha,\beta,\gamma\in[N]} \widetilde{\mathcal{Q}}^{+-}_{\alpha\beta}\ \langle \boldsymbol{\psi}^t_{-\gamma}, \boldsymbol{\psi}^0_\alpha\rangle \langle \boldsymbol{\psi}^0_\beta, \boldsymbol{\psi}^t_{\gamma}\rangle \\ &= \sum_{\alpha,\beta,\gamma\in[N]} \widetilde{\mathcal{Q}}^{+-}_{\alpha\beta}\ \langle \boldsymbol{\psi}^t_{-\gamma}, \boldsymbol{\psi}^0_\alpha\rangle \langle \boldsymbol{\psi}^0_{-\beta}, \boldsymbol{\psi}^t_{-\gamma}\rangle \end{aligned}$$

where we used particle-hole symmetry in the last step. Similarly for its Hermitian conjugate, but now only $\langle\hat{d}^\dagger_i\hat{d}^\dagger_j\rangle$ with $i \in [N]$ and $j \in [-N]$ it is trivial to show that it is identical to the above. Thus we finally obtain:

$$\hat{U}^\dagger\hat{Q}\hat{U} - \frac{1}{2}\operatorname{Tr}\mathcal{Q}_e + \frac{1}{2}\operatorname{Tr}\Big\{\widetilde{\mathcal{Q}}_{++}\Big\} = \langle\Omega|\hat{A}(t)|\Omega\rangle + 2\,\langle\Omega|\hat{B}(t)|\Omega\rangle$$

and the net change of the observable over time (conveniently, the right hand side is zero at $t = 0$) is:

$$\langle\hat{Q}(t)\rangle - \langle\hat{Q}(0)\rangle = \sum_{\alpha,\gamma\in[N]}\sum_{\beta\in\mathbb{Z}^*_N} \widetilde{\mathcal{Q}}_{\alpha\beta}\ \langle \boldsymbol{\psi}^t_{-\gamma}, \boldsymbol{\psi}^0_\alpha\rangle \langle \boldsymbol{\psi}^0_\beta, \boldsymbol{\psi}^t_{-\gamma}\rangle$$

where remarkably, the sum over β covers the entire energy spectrum, the sum over α only the positive part and γ only the negative part. Also note that the factor $1/2$ from the BdG redundancy is not present anymore. For better readability:

$$\langle\hat{Q}(t)\rangle - \langle\hat{Q}(0)\rangle = \sum_{\alpha\in[N]}\sum_{\beta\in\mathbb{Z}^*_N}\sum_{\gamma\in[-N]} \langle\gamma^t|\alpha^0\rangle\langle\alpha^0|\hat{Q}|\beta^0\rangle\langle\beta^0|\gamma^t\rangle\,. \tag{5.9}$$

We will see that this operator converges much better when one substitutes N by some $N_{\text{cutoff}} < N$ and is representative of the actual cut-off in energy with respect to the Fermi level.

■ Chapter VI
Signatures of braiding

In this chapter, the measurement of current-density at the exit of the superconductor is addressed. This is the only way of locally observing whether braiding has taken place inside the superconductor beforehand. The dynamical exit current density is studied here and we conclude which regime is best suited for the detection of braiding.

1. Adiabatic crossings and diabatic transitions

1.1. Domain wall in terms of overlaps

We analyze the edge-vortex excitations. The time-evolution of a single excitation can be written in terms of the initial eigenbasis:

$$|\beta^t\rangle = \sum_{\alpha=1}^{2N} \mathcal{U}_{\alpha\beta} \, |\alpha^0\rangle \tag{6.1}$$

with $\mathcal{U}_{\alpha\beta} = \langle\alpha^0|\hat{U}(t)|\beta^0\rangle$. In Fig. VI.1 we represent the values of $\mathrm{Re}\{\mathcal{U}_{\alpha\beta}\}$ for the lowest energy edge mode. The π-jumps in the overlap represent the position of the edge-vortices. A similar behaviour can be found in higher energy excitations, which contain nonzero dynamical phases and couple more with the junction.

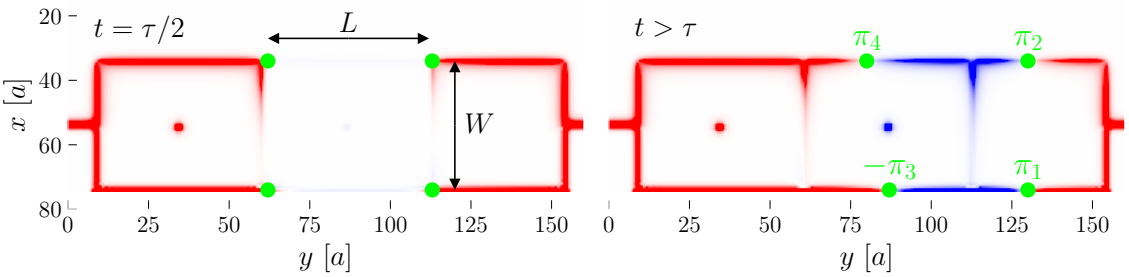

Figure VI.1: Local overlap $\mathrm{Re}\{\mathcal{U}_{\alpha\alpha}(t)\}$ for the lowest energy edge state (summed with vortices for the sake of representation) at two different times. (Left) during the injection which occurs around $\varphi = \pi$ or values of t around $\tau/2$. (Right) After the injection the π-domain walls (in green) represent the edge-vortices which fuse at the exit of the superconductor. Here $\tau = 75a/v$.

1.2. Global $E = 0$ crossing of the edge states

We represent the values of the overlap with instantaneous eigenstates of $H_{\mathrm{BdG}}(\varphi)$ (denoted by $|\alpha^\varphi\rangle$) with the size of the dots in Fig. VI.2, in a system where the junction width is $W = 40a$ and the characteristic time is $\tau = 200$ $[a/v]$. The discretization of momentum results in a high folding of the Brillouin zone thereby making making the spectrum dense around zero energy and generating an important number of avoided crossings. Thus, under a linear time-evolution, diabatic transitions

occur necessarily. In the leftmost plot, the fermionic pair of bulk vortices slightly below zero energy evolves towards its counterpart at a slightly positive energy. This unambiguously corresponds with a change in parity since it is an adiabatic crossing isolated from other states.

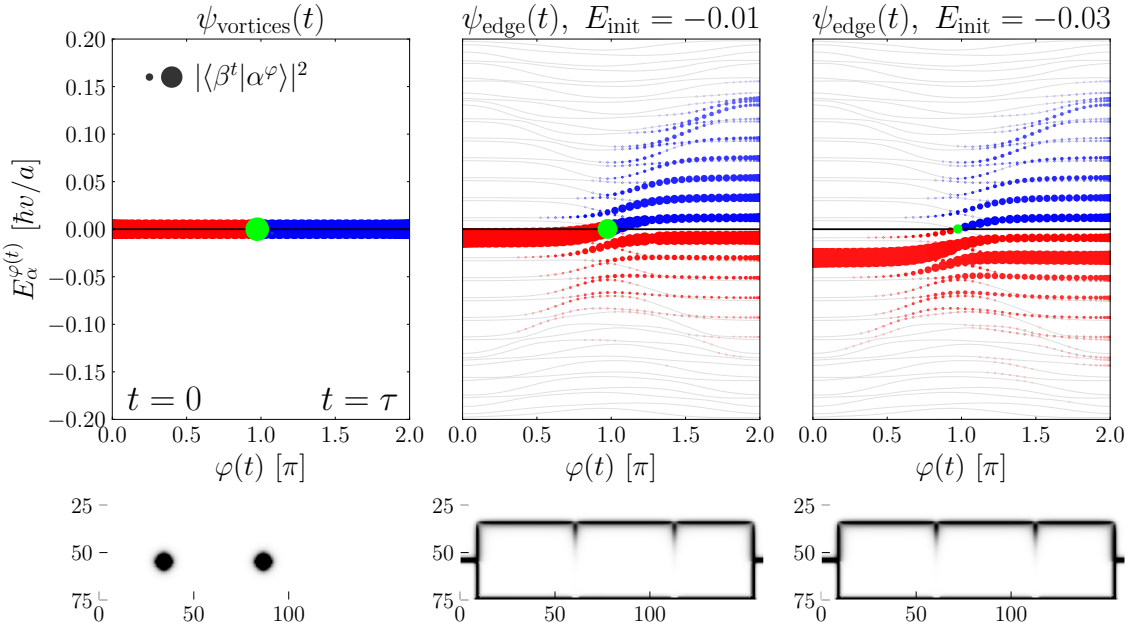

Figure VI.2: Instantaneous spectrum of $\mathcal{H}_{\text{BdG}}(\varphi)$ (gray curves) and squared overlap of an evolved state – ψ_{vortices} or ψ_{edges}– with instantaneous eigenstates $|\alpha^\varphi\rangle$ (size of the dots). Positive (negative) states are shown in blue (red), and dynamical crossings with zero energy are represented by a green dot. The bottom shows the wave function amplitudes at $t = 0$ for these energies. System with $W = 40a$ and $\tau = 200a/v$.

Now turning to the lowest edge mode excitation in the middle plot, it spreads across the spectrum throughout the evolution. In particular, the crossing through zero energy event cannot be isolated; it occurs in a large number of different excitations as well. This is for example shown in the rightmost plot. This begs for a more elaborate description of the parity exchange for which we refer to Ch. VII.

Finally, note that near $\varphi = \pi$ the effect of the gap closing inside the Josephson junctions is visible on the entire spectrum. This is indeed visible on a scale which corresponds with the effective gap in the junction $\Delta_0 = 0.116\ \hbar v/a$ and it is the only variable energy scale in the system as anticipated previously [18]. Second, one notes the (adiabatic) band crossings observed between $\varphi \in [\pi, 3\pi/2]$. In fact, at higher states they correspond with states localized at each opposite edges of the junction. It is clear that the junction lowers the energy of one edge state more than the other (this comes from the fact that the junction is entirely in the topological phase). After this process, the state at one edge finds itself exchanged with the opposite edge as their respective bands were inverted.

1.3. Forbidden transition without vortices

In the absence of vortices, the gap inversion cannot imply a change of parity for the edges, unless the edges can exchange parity with the bulk. It seems more likely that both gap inversions will only affect the edge. We consider this situation

in Fig. VI.3. Clearly, the tendency of the system is not to cross the $E = 0$, which indicates that the parity remains the same. The lowest energy state does not cross the $E = 0$ level at all during the process and globally stays at $E = -10^{-7}$ in amplitude. On the right side we show the two lowest energy excitations, which correspond with the two respective edge states. With the gap inversion, these states most remarkably do cross the $E = 0$ level, and end up in an equal superposition of the lowest energy states at energies $\pm 10^{-7}$ (shown in green). This suggests that, despite the fact that we do not see an overall transition through the $E = 0$ level, the injection process at both junction has produced Majorana-zero modes in the zero energy subspace.

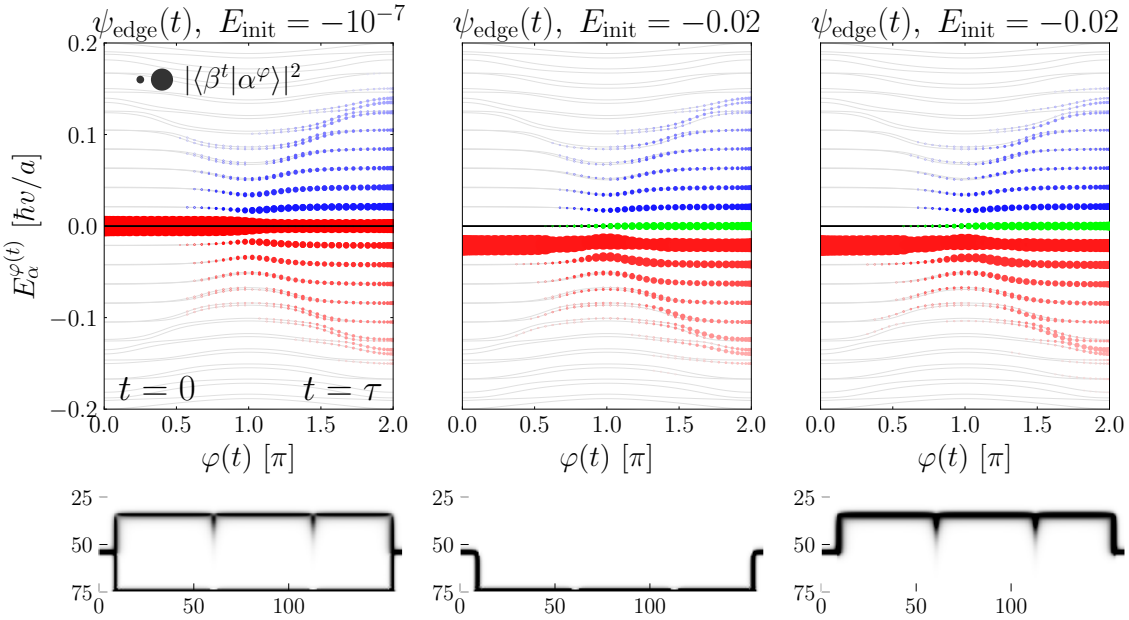

Figure VI.3: Instantaneous spectrum of $\mathcal{H}_{\text{BdG}}(\varphi)$ (gray curves) and squared element of the evolution matrix *without vortices*. Here the green state is one where the evolved state is in an equal amplitudes superposition of the states at $\pm 10^{-7}\hbar v/a$. The bottom shows the wave function amplitudes at $t = 0$ for these energies. System with $W = 40a$ and $\tau = 200a/v$.

2. Convergence of charge

Before analyzing the current density at the exit of the system, we address the methodical point developed in Cha. V namely the evaluation of the current density in the electron-hole basis in (5.7) or in the spectral decomposition of stationary states (5.9). In Fig. VI.4 we show the convergence of each method as a function of the cutoff energy E_{cutoff}. The operator evaluated is the local current density $\rho = -\tau_z\sigma_y\hat{\text{proj}}_{y_{\text{exit}}}$ at the exit of the superconductor (contained in the projector). We then define the quantities:

$$I(t) := \langle\hat{\rho}(t)\rangle - \langle\hat{\rho}(0)\rangle$$
$$Q(t) := \int_0^t I(s)\mathrm{d}s$$

and denote by $Q(\infty)$ the value of $Q(t)$ after the quench. The system used here has $W = 40a$, $L = 40a$ and $\tau = 350a/v$. It is immediately clear that the eigenbasis

method results in a much more stable convergence. It is still worth noting that the oscillation in energy seen in the electron-hole basis are associated with the bound states in the junction. Indeed, they only appear at energies higher than Δ_0. In fact, it was seen that the frequency of these oscillations is controlled by the width W of the junction; they become more frequent with increasing W, which shows that an increasing number of excitations populate the junction for a fixed energy range as W is increased. One might therefore expect that, in the absence of bound states, the electron-hole decomposition of charge works reasonably well.

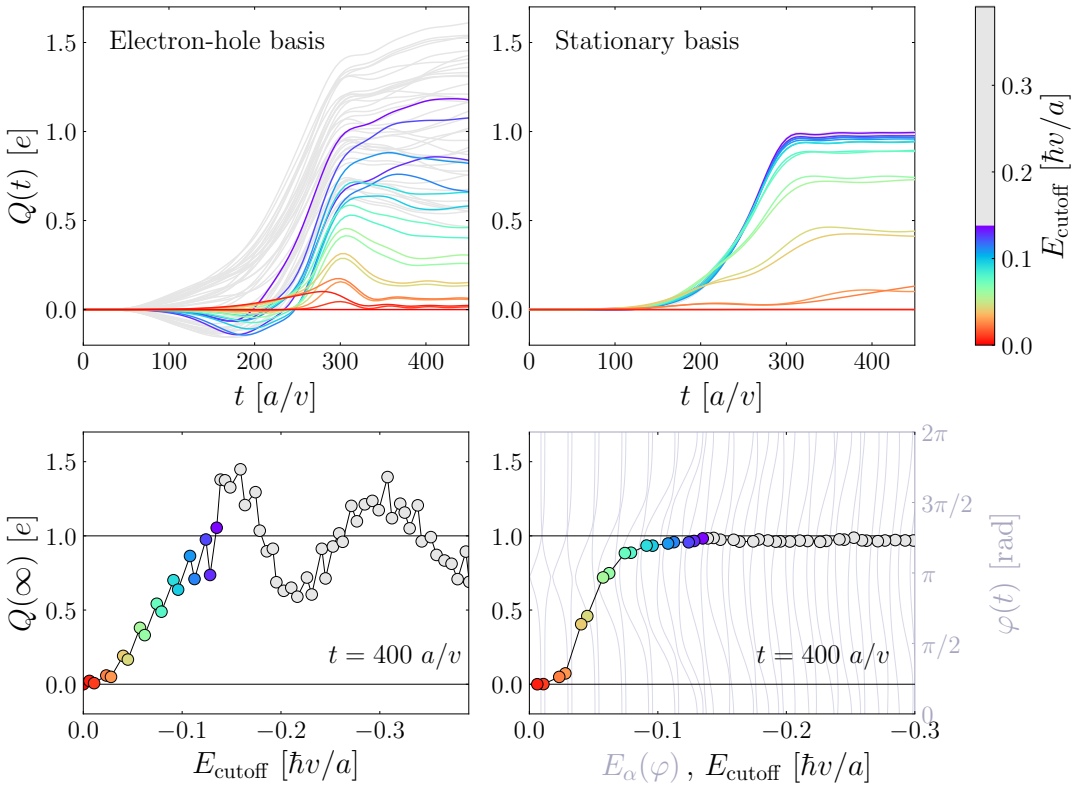

Figure VI.4: Evaluation of the net charge increase as a function of the energy cutoff in the (Left) electron-hole basis and (Right) stationary basis methods. The convergence is shown as a function of time (Top), and the final converged value $Q(\infty)$ as a function of energy too (Bottom). We also show the bands as a function of φ of a related system in the right plot.

3. Quantization of charge

As observed in the previous convergence plot, it is possible to reach a quantized value of charge dynamically. We consider a number of different limits in which the theoretical result is obtained.

3.1. Time-separated current pulses

First, consider the limit where the the junction separation is large L compared to the injection time. We consider the system with $L = 350a$, $\tau = 300a/v$ and $W = 25a$. Thus the estimated injection time is $t_{\rm inj} = 103a/v$. The simulated net current density and charge are shown in Fig. VI.5 along with the theoretical prediction from (2.3) (dashed lines). The similarity with the simulation is remarkable in the case with and without vortices, in terms of current and in terms of quantized

charge which produces values of $\pm e/2$. It is clear that the presence of vortices only affects the second pair of edge-vortices as expected.

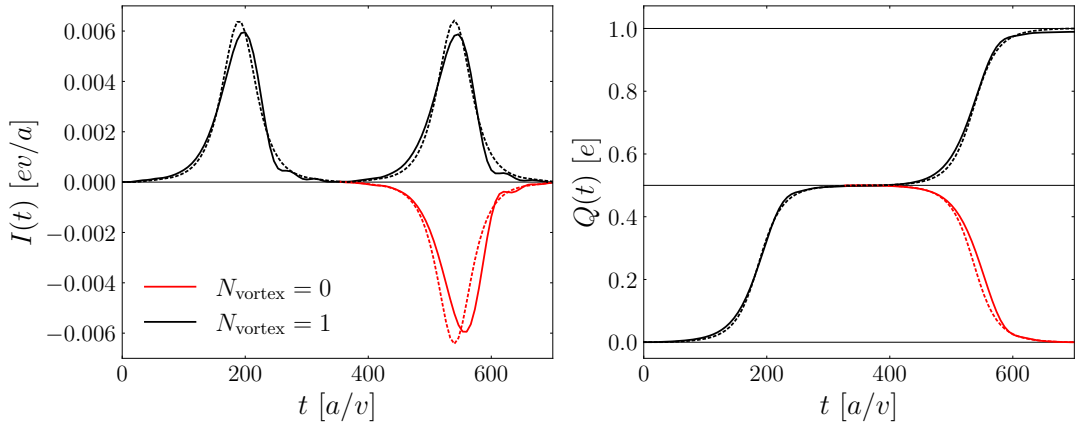

Figure VI.5: Local current density pulses (left) and integrated local current density pulse (right) at the exit of the superconductor, where the distance $L = 350a$ between the injection events is large compared to the duration of the injection $vt_{\text{inj}} = 103a$. Both numerical (solid lines) and analytical (dashed lines) results are shown for the cases with (black) and without (red) vortices. Time origin is arbitrary.

3.2. Merging into a single pulse

Now progressively changing the inter junction distance L until the charge pulses are merged is done in Fig. VI.6. Here we recover the theory from Ref. [18] of a single pulse achieved by close junctions. Nevertheless the current shows some deviation from the theory in its shape; it is not symmetric. This could for example be caused if the second pair of edge-vortices experienced the junctions differently than the first pair.

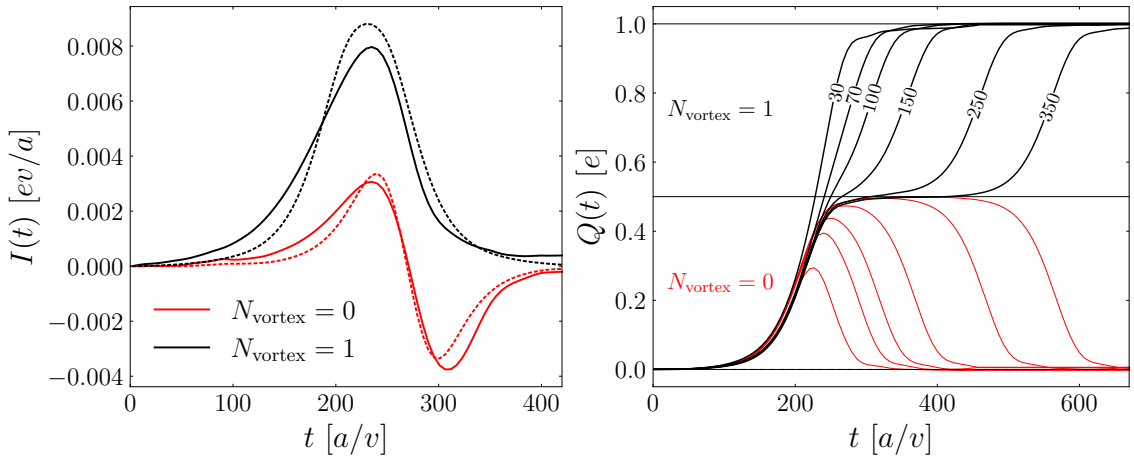

Figure VI.6: Net current density (left) and accumulated charge (right). The charge is shown for different values of L (in units of a) shown on top of the lines. Here $vt_{\text{inj}} = 103a$ and the time origin is arbitrary.

4. Path-length difference effects

In Ref. [22] the effect of path-length difference between the fusing vortices on the quantization of charge was studied. As one expects, if the edge-vortices arrive

at the exit with a relative time-delay, their fusion cannot produce unit charge.

The system studied here naturally contains path-length differences. The differences in localization length between the edges (see Sec. 2.3 of Ch. III) induces a small path-length difference between the top and bottom edges (namely, at corners the edge with the largest localization length "cuts" the corners). The main contributor to path-length differences is the junction, which is a topological insulator such that only the top edge may penetrate far in the junction at most values of φ. Finally, the top edge states hybridize with the junction at higher energies. This is shown in Fig. VI.7 on the right where velocity expectation values are calculated as a function of energy in a short system where this effect is exacerbated. The latter is a minor consideration since this is not the actual velocity of the edge state; all states on the edge have velocity v. These three mechanisms combined result in a small path-length being present in the system, which can be neglected for large enough τ as we have done so far. For illustration the local complex phase of the top (denoted χ_2) and bottom (χ_1) edge fermions is shown in Fig. VI.7. The phase is evaluated near the exit of the superconductor so that both π jumps are observed. This corresponds with the $\tau = 20a/v$ case and the energy of the shown state is $E = -0.08\hbar v/a$ which is below the effective gap Δ_0. It is clear that the junction only affects the phase of the top edge χ_2. We come back to the related effects in the next subsection.

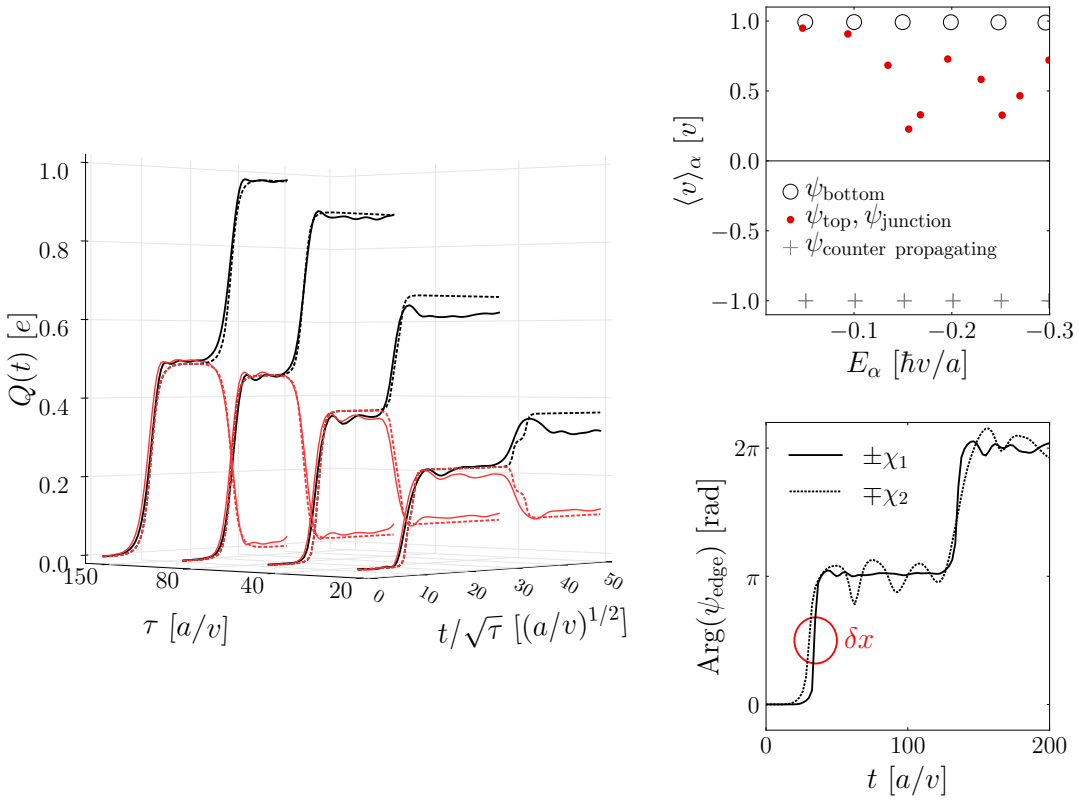

Figure VI.7: (Left) Quantization of charge with (black) and without (red) vortices simulated for $\tau v/a = 20, 40, 80, 150$ (solid lines). Predictions with an estimated path-length are shown with dashed lines. (Top right) Expectation value of velocity for the single particle states. The top edge and junction states are hybridized so their velocity expectation is lowered. (Bottom right) Local phase of the wave function for $\tau = 20a/v$ near the exit of the superconductor at both edges χ_1 and χ_2 at an energy below the effective gap Δ_0.

The constant path-length difference is used to our advantage here to study its effect on quantization. By increasing the time τ and considering the constant path-length difference δx, the ratio δ_x/vt_{inj} will decrease, thus improving the quantization of charge. We consider $v\tau/a = 20, 40, 80, 150$ (higher values here recover the theory discussed above) for a junction length $W = 25a$ as before so the estimated injection times are $vt_{\text{inj}}/a = 7, 14, 28, 52$ respectively. Finally, the inter junction distance L is taken to be equal to $v\tau$ so that the pulses are separated in time. The results are shown in Fig. VI.7 (left) with and without vortices. The theoretical expectation (2.4) was shown with dashed lines. For the theoretical expectation, it was assumed that $\delta x = 7a$ for the first pulse based on the inspection of the phase and on the goodness of the fit. This is of the same order as the injection time for the case $\tau = 20a/v$. Clearly, the theoretical expectation matches the simulation for the first plateau below $e/2$ for all values of τ, whereas the theoretical expression was evaluated at a constant δx. This strongly suggests that path-length difference governs the charge quantization here and that the accumulated path-length by the first pair of edge vortices is indeed constant. For the second pulse however, a variable path-length was used of $\delta x/a = 7, 10, 11, 13$ for $\tau v/a = 20, 40, 80, 150$ respectively to accommodate with the theory. This suggests that faster injections exacerbate path-length difference effects for the second pair of edge vortices which passes near both junctions. Finally, note the discrepancy between the case with and without vortices for the second pulse, where a small drop is seen after reaching the quantized value. In the next section, we explore the possibility of higher order interference effects due to the junction.

5. High order interference

In this section the role of the bound states in the junction is investigated. The existence of bound states is expected above the gap Δ_0. At subgap energies, the edges may not couple through the junction at $\varphi = 0$. This is shown in the wave function amplitude in Fig. VI.8. Above the gap however, the junction allows for bound states to exist, which couple both edges at higher energies. Different modes of the junction are shown in Fig. VI.8.

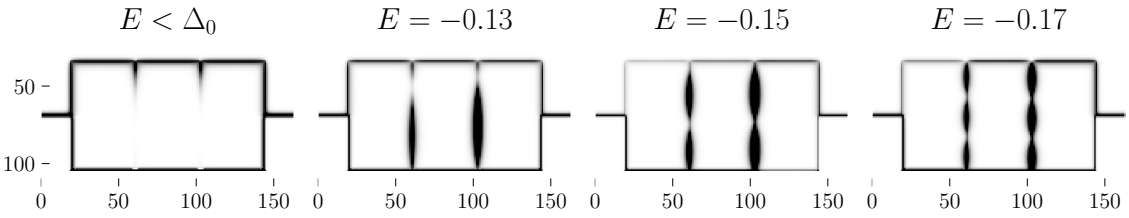

Figure VI.8: Wave function amplitudes of negative energy excitations at $t = 0$ for different energy values shown in units of $\hbar v/a$. The leftmost state is at $E = -0.07$. The system shown corresponds with $W = 70a$.

The junction may be populated by increasing its width W. This will simultaneously reduce the injection time however, so τ is chosen such that the estimated injection time t_{inj} remains constant. In Fig. VI.9, the local current density is shown for two estimations of the injection time and for five values of the junction length W. The estimation of the injection time is reasonable since the main peaks have

approximately the same width given an injection time. The discrepancies seen in charge quantization which could not be accounted for by the theoretical expressions are attributed to higher order interferences. The oscillations in charge produced after the injection indeed suggest that the bound states in the junction were excited. In fact the period of these oscillations – for the $t_{\text{inj}} = 40a/v$ case – have a period of approximately $T = 50a/v$. This corresponds with a characteristic energy $E = \hbar 2\pi/T \approx 0.13\ \hbar v/a$ which is the energy of the lowest bound state of the junction. The fundamental period seen in the case $t_{\text{inj}} = 10a/v$ is also around $50a$. However, the signal contains higher frequencies as well, which we attribute to the excitation of higher energy bound states at shorter injections. Finally, these oscillations tend to be suppressed as W is decreased as shown in the case of $t_{\text{inj}} = 40a/v$. They are completely suppressed at large values of τ as shown in the ideal results of Sec. 3. The use of a point junction eliminates this consideration altogether. One should note that the effect of these high order oscillations on the plateau values $Q(\infty)$ is small, as observed in Fig. VI.7 before. The same interference were observed in the absence of vortices, which suggests that this behavior is a characteristic of the junctions rather than that of vortices.

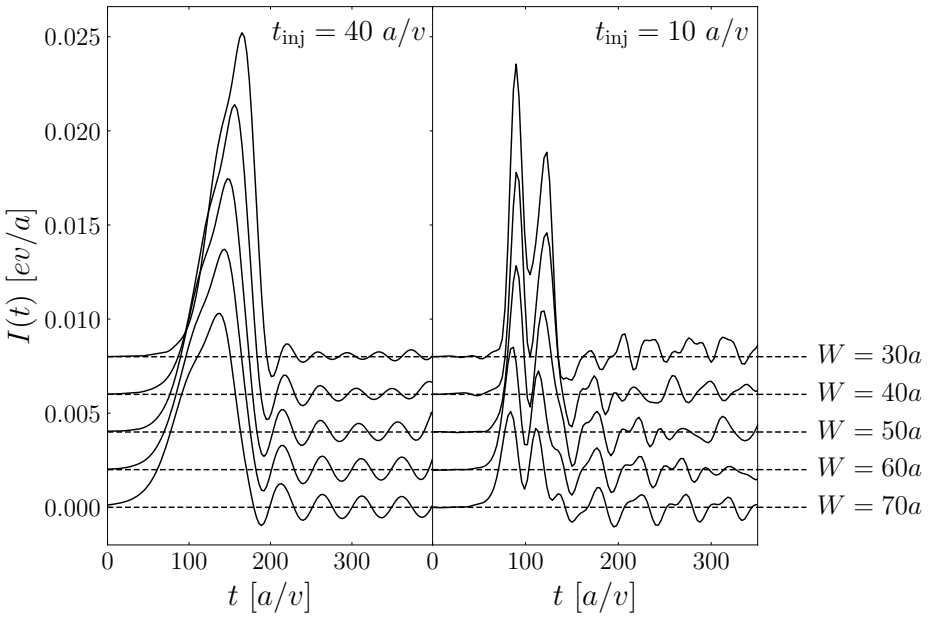

Figure VI.9: Current density at the exit of the superconductor, with variable junction length W shown on the right, for two estimated injection times $t_{\text{inj}} = 40a/v$ (Left) and $t_{\text{inj}} = 10a/v$ (Right). Thus $\tau = \Delta_0 W t_{\text{inj}}$ was used in the simulations. The origin $I(t) = 0$ is shifted according to the dashed lines for different W for the sake of representation, so that the values of $I(t)$ on the vertical axis correspond with the origin at 0.

■ Chapter VII
Parity protection of the edge-vortex

Thus far, braiding was only discussed through its signature in charge. The edge-defects produced in the junction are expected to carry the parity qubit of the bulk vortices. After escaping into the edges, they propagate to the exit, as studied before. Here, we address the question whether the edge-vortices carry the parity lost by the bulk. Because this part is still a work in progress, results are at an early stage. We first present a method which is true in some approximation. The second section presents an exact approach currently studied in parallel.

1. Fermi-sea picture

1.1. Introduction

Parity protection above the ground state.— If we denote the Majorana operators by π_i for the edge-vortex zero modes and γ_i for the bulk vortices – identical to the convention in Fig. I.2 – then the parity operator of the vortices and bulk vortices in the idealized description is given by:

$$\hat{P} = i\gamma_1\gamma_2 \cdot i\pi_1\pi_2 \cdot i\pi_3\pi_4$$

which holds for an infinitely long junction and infinite time; under these conditions the braiding process takes place entirely in the ground state manifold and:

$$i\gamma_1\gamma_2 \cdot i\pi_3\pi_4 \to (-i\gamma_1\gamma_2) \cdot (-i\pi_3\pi_4)$$

describes the braiding process. The total parity is conserved but each pair gains a different parity. In the non-idealized theory however, the edge-vortices are excitations above the ground state and the zero-modes contain fermionic excitations (albeit without interacting with them). One can prove that leaving the ground state does not compromise parity protection under these conditions [55] and that instead, we consider the edge-vortex as the total edge collection i.e.:

$$\hat{P} = i\gamma_1\gamma_2 \cdot \hat{P}_{\text{edge}} \to (-i\gamma_1\gamma_2) \cdot (-\hat{P}_{\text{edge}})$$

is the total parity of the excited state. Note that $\hat{P}_{\text{edge}}$ also contains π_1 and π_2 so one cannot separate the two pairs of edge-vortices anymore; local contributions to the parity along the edge cannot be treated trivially.

Parity operator.— As mentioned in Ch. I, a Bogoliubov quasiparticle is a parity-conserving excitation. Therefore, the parity of BdG excitations is the electronic parity so that the following formulations of the parity operator are equivalent:

$$\hat{P} = (-1)^{\hat{n}} = \prod_{i=1}^{N}(1 - 2\hat{c}_i^\dagger\hat{c}_i) = \prod_{\alpha=1}^{N}(1 - 2\hat{d}_\alpha^\dagger\hat{d}_\alpha)$$

where $\hat{n}$ is the electron number operator. In our description, the vortices are also calculated in a fermionic basis, so that the eigenstate which contains the vortices has a well defined parity. Note that when applied on the ground state $|\Omega\rangle$ this operator always gives 1, which is the initial ground state parity (up to a minus sign). For future reference we expand the product of the operator in a sum of ordered sums:

$$\begin{aligned}\hat{P} &= 1 - 2\sum_{i_1} \hat{d}^\dagger_{i_1}\hat{d}_{i_1} + 4\sum_{i_1<i_2} \hat{d}^\dagger_{i_1}\hat{d}_{i_1}\hat{d}^\dagger_{i_2}\hat{d}_{i_2} - 8\sum_{i_1<i_2<i_3} \hat{d}^\dagger_{i_1}\hat{d}_{i_1}\hat{d}^\dagger_{i_2}\hat{d}_{i_2}\hat{d}^\dagger_{i_3}\hat{d}_{i_3} + ... \\ &= 1 + \sum_{\alpha}^{N}(-2)^\alpha \sum_{i_1\leq ...\leq i_\alpha} \hat{d}^\dagger_{i_1}\hat{d}_{i_1}\hat{d}^\dagger_{i_2}\hat{d}_{i_2}...\hat{d}^\dagger_{i_\alpha}\hat{d}_{i_\alpha} \end{aligned} \tag{7.1}$$

so that we only treat products of $\hat{d}_\alpha$ operators. Furthermore, this product can be normal ordered using anti-commutation relations.

1.2. Time-dependent parity expectation

Approximation.— The approach essentially consists of "counting" the parity of the evolved quasiparticles as seen from the stationary quasiparticles from the bottom or top parts of the spectrum. By adopting the Fermi sea picture introduced in Sec. 3.3 of Ch. IV we use the vacuum $|\text{vac}\rangle$ annihilated by the negative energy annihilation operators (or positive energy creation operators) so that the time-evolved state is:

$$\hat{U}(t)\,|\Omega\rangle = \prod_{\alpha\in[-N]} a^\dagger_\alpha(t)\,|\text{vac}(t)\rangle$$

where we denoted $|\text{vac}(t)\rangle := \hat{U}(t)\,|\text{vac}\rangle$ so the ground state parity is:

$$\langle\hat{P}(t)\rangle = \langle\Omega|\,\hat{U}^\dagger(t)\hat{P}\hat{U}(t)\,|\Omega\rangle\,.$$

We now present a demonstration which relies on the assumption that this vacuum is still the same vacuum under time evolution: $\hat{d}^\dagger_\alpha\,|\text{vac}(t)\rangle = 0\;\forall\alpha\in[N]$ or $\hat{d}_\alpha\,|\text{vac}(t)\rangle = 0\;\forall\alpha\in[-N]$. I.e. the state filled with all positive energy excitations – when evolved – is still a vacuum for a stationary positive energy excitation. At $t = 0$, this assumption is naturally correct but at $t > 0$, it may seem reasonable but since we will consider truncated values of N this is difficult to assess.

Application of exchange rules.— Let us consider the parity operator expressed in terms of $\hat{d}^\dagger_\alpha$, $\alpha\in[-N]$. Then consider the exchange rule between a stationary state $\hat{d}_\alpha$ and an evolved state $\hat{a}^\dagger_\beta$ with $\alpha,\beta\in[-N]$. Then their exchange rule is given by the anti-commutator:

$$\{\hat{d}_\alpha,\hat{a}^\dagger_\beta\} = \sum_{\gamma\in\mathbb{Z}^*_N} \mathcal{U}_{\gamma\beta}\{\hat{d}_\alpha,\hat{d}^\dagger_\gamma\} = \mathcal{U}_{\alpha\beta}(t) \tag{7.2}$$

where we used the quadratic evolution between $\hat{d}$-operators, with $\mathcal{U}_{\alpha\beta} := \langle\alpha^0,\beta^t\rangle$ the overlap. Note that this expression correctly takes care of the redundancy. Furthermore, one has to be careful with the fact that $\{\hat{d}_\alpha,\hat{a}^\dagger_\beta\}\neq\{\hat{d}_\alpha,\hat{a}^\dagger_\beta\}^\dagger$. Then we calculate all the k-th order terms of the expansion (7.1) as:

$$\langle\text{vac}(t)|\left(\prod_{\alpha\in[-N]} a_\alpha\right)\left(\prod_{\beta\in[-k]} \hat{d}^\dagger_\beta\hat{d}_\beta\right)\left(\prod_{\alpha\in[-N]} a^\dagger_\alpha\right)|\text{vac}(t)\rangle \tag{7.3}$$

where the leftmost product is ordered the opposite of the rightmost product. Then, using the exchange rule (7.2) it is possible to "normal order" the entire expression: bringing all terms $\hat{d}_\beta$ to the far right and all $\hat{d}^\dagger_\beta$ to the far left. If the parity operator is expressed in positive energy eigenstates, the procedure is entirely equivalent, but the terms must be anti-normal ordered. We show the details of the derivation in the next subsection, for now this yields:

$$\langle \hat{P}(t) \rangle = \sum_{K=0}^{N} (-2)^K \sum_{i_1<\ldots<i_K} \sum_{\alpha_1<\ldots<\alpha_K} \left| \sum_{\mathcal{P}} \mathrm{sgn}_{\mathcal{P}} \mathcal{P}(\mathcal{U}_{i_1\alpha_1} \ldots \mathcal{U}_{i_K\alpha_K}) \right|^2 \tag{7.4}$$

where $\mathcal{P}$ denotes the set of all permutations of the product of terms in the overlap matrix.

Complexity and truncations.— Before evaluating the above we note its factorial complexity due to the two ordered sums of permutations of increasing order:

$$\mathcal{O}\left(0!\binom{N}{0}^2 + 1!\binom{N}{1}^2 + 2!\binom{N}{2}^2 + \ldots + N!\binom{N}{N}^2\right) = \mathcal{O}\left((N/2)!\binom{N}{N/2}^2\right).$$

Thus, we are looking for a way to truncate the expression. The first truncation we introduce is that over N: the number of states included in the calculation, which we denote N_{cutoff}. If we consider the bottom part of the spectrum - where we evolve all the states – the expression is highly problematic, because each state evolves to a number of neighboring states which need to be exchanged. In terms of the positive part of the spectrum the truncation is much more reasonable. The second truncation one can make is the order of the product of overlaps which we denote k. One might expect that k is related to the number of dynamical crossings, so that this approximation will work for slow evolutions.

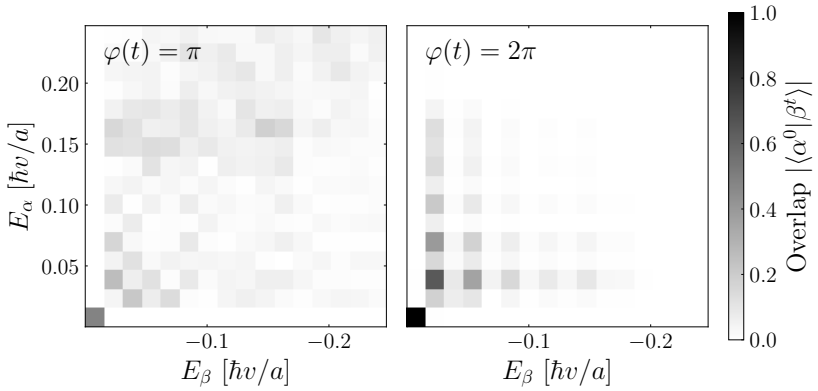

Figure VII.1: Overlap matrix $\mathcal{U}_{\alpha\beta}(t)$ absolute values for $\alpha \in [N]$ positive energy eigenstates and $\beta \in [-N]$ negative energy evolved states, at two values of $\varphi(t)$ at $t = 250a/v$ and $t = 500a/v$.

Parity evolution.— We consider a system with a long junction $W = 50a$ and with $\tau = 500a/v$. We minimize the length of the system as much as possible to minimize the number of states in the discretization. Then the overlap matrix between the positive energy eigenstates and the evolved negative energy eigenstates is shown in Fig. VII.1. On the left in the middle of the injection, the energy range is large

which shows the extent to which the bands are lowered. At the end of the evolution, only a select range of states has a nonzero overlap with the eigenstates as shown in the right figure. A checkerboard pattern is observed in the matrix, where we clearly see that states from one edge χ_1 have evolved into the other edge χ_2, which is in agreement with what was observed in Fig. VI.2. Furthermore, the vortex state is completely isolated in energy from the other states, as expected.

We now evaluate equation (7.4) numerically at 50 values of time corresponding with $\varphi(t) \in [0, 2\pi]$ using overlap matrices as the ones in Fig. VII.1. The result is shown in Fig. VII.2 (left). In the case where $N_{\text{cutoff}} = 1$ only the vortex state is included. The vortex changes in parity very clearly. N_{cutoff} is then increased in the approximation of $k = 5$ order terms, such that it includes a range of energy excitations of the edges, until the parity expectation returns to even. This establishes that no parity is lost in the states of the bulk and that all states contributing are near Δ_0. The bound states in the junction are also included. However, it is not clear at this moment if the contribution comes from the bound state or from the edges, since these states are hybridized junction and edge states. Thus we are currently studying:

$$\hat{P} = i\gamma_1\gamma_2 \cdot (\hat{P}_{\text{edge}}\hat{P}_{\text{junction}}).$$

It is possible to project out the junction positions from the overlaps in order to verify this further, which we do not present here. Note that the recovered value is not exactly one, as observed in Fig. VII.2 (right) which seems to have reached convergence. This is still under investigation and the case without vortices is also under investigation. Also note that curiously the parity switch does not occur at $\phi = \pi$. This could be attributed to asymmetries in the system which were observed separately in the adiabatic bands as well, where the crossing occurs for values of $\varphi > \pi$.

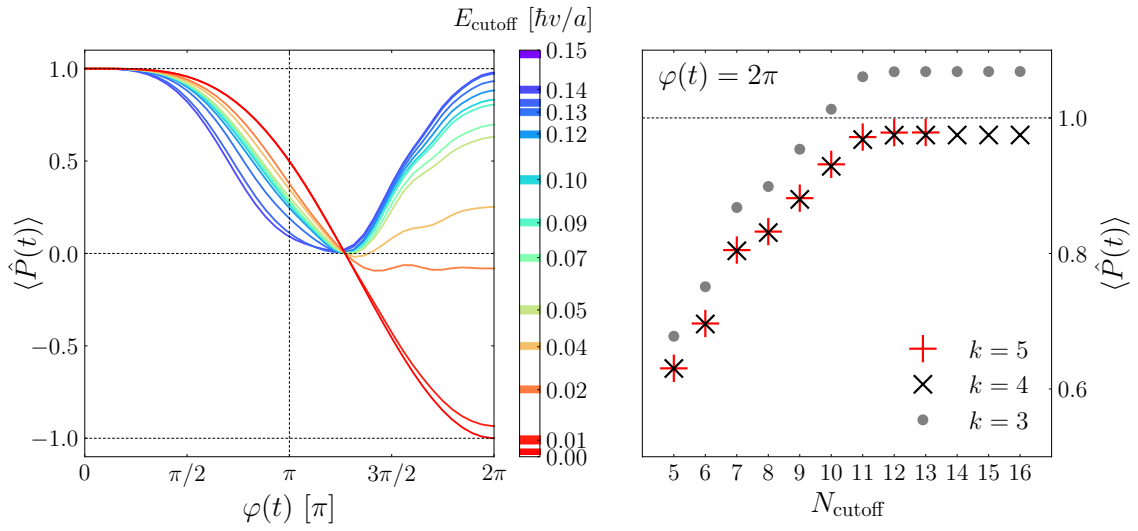

Figure VII.2: (Left) Time evolution of the parity expectation value for different values of N_{cutoff} here shown in energy. Here 12 edge excitations are added to compensate for the parity loss in the vortices. (Right) Convergence of parity as a function of N_{cutoff} and the order of products k.

1.3. Calculation details

Let us consider the expression (7.3) with the first order $k = 1$. The right side acting on the ket is then simply given by:

$$\begin{aligned}\hat{d}_1 \prod_\alpha \hat{a}^\dagger_\alpha |\text{vac}\rangle &= (\{\hat{d}_1, \hat{a}^\dagger_1\} - \hat{a}^\dagger_1 \hat{d}_1)\hat{a}^\dagger_2 ... \hat{a}^\dagger_N |\text{vac}\rangle \\ &= \mathcal{U}_{11} \prod_{x\neq 1} \hat{a}^\dagger_x |\text{vac}\rangle - \mathcal{U}_{12} \prod_{x\neq 2} \hat{a}^\dagger_x |\text{vac}\rangle + ... \\ &= \sum_\alpha (-1)^\alpha \mathcal{U}_{1\alpha} \prod_{x\neq\alpha} \hat{a}^\dagger_x |\text{vac}\rangle \,.\end{aligned}$$

Here the product state on the right is removed each state which was exchanged into the evolution matrix. The left side acting on the bra is exactly the Hermitian conjugate, and because all the states in the above sum are mutually orthogonal we obtain the first order estimation of $\langle \hat{P}(t)\rangle$:

$$\langle \hat{P}(t)\rangle = 1 - 2\sum_{i_1}\sum_\alpha |\mathcal{U}_{i_1\alpha}|^2 + ... \,.$$

Note that this approximation so far only makes sense for a single particle in the ground state. If this particle is evolved into any orthogonal state, the parity goes from odd to even. If the overlap remains constant in time, the parity remains odd. This approximation is completely false when one considers more than one particle. For second order terms, note that $\hat{d}^\dagger_1 \hat{d}_1 \hat{d}^\dagger_2 \hat{d}_2 = \hat{d}^\dagger_1 \hat{d}^\dagger_2 \hat{d}_2 \hat{d}_1$ and:

$$\begin{aligned}\hat{d}_2 \hat{d}_1 \prod_\alpha \hat{a}^\dagger_\alpha |\text{vac}\rangle &= \sum_\alpha (-1)^\alpha \mathcal{U}_{1\alpha}\ \hat{d}_2 \prod_{x\neq\alpha} \hat{a}^\dagger_x |\text{vac}\rangle \\ &= \sum_{\alpha\neq\beta} (-1)^{\alpha+\beta+\mathbb{1}_{\beta>\alpha}} \mathcal{U}_{1\alpha}\mathcal{U}_{2\beta} \prod_{x\neq\alpha,\beta} \hat{a}^\dagger_x |\text{vac}\rangle\end{aligned}$$

where $\mathbb{1}_{\alpha>\beta}$ is an indicator function which is one if $\alpha > \beta$ and zero else. It arises because the number of permutations to achieve normal ordering will differ by one depending on whether $\hat{a}^\dagger_\alpha$ was already excluded from the product state or not, which results in a sign flip if $\beta > \alpha$. The key idea is that we want to write this sum as a linear combination of different mutually orthogonal states. This is not the case here since the same state is present on the right e.g. when $\alpha = 1, \beta = 2$ and $\alpha = 2, \beta = 1$ with coefficients $\mathcal{U}_{11}\mathcal{U}_{22}$ and $-\mathcal{U}_{12}\mathcal{U}_{21}$ respectively. Those two states differ by a minus sign because in one case $\beta > \alpha$ which in other terms is a manifestation of the anti-symmetrization condition. This is resolved by splitting the sum in two parts:

$$\begin{aligned}&\sum_\alpha (\sum_{\beta<\alpha} + \sum_{\beta>\alpha})(-1)^{\alpha+\beta+\mathbb{1}_{\beta>\alpha}} \mathcal{U}_{1\alpha}\mathcal{U}_{2\beta} \prod_{x\neq\alpha,\beta} \hat{a}^\dagger_x |\text{vac}\rangle \\ =&\left[\sum_{\alpha>\beta} (-1)^{\alpha+\beta} \mathcal{U}_{1\alpha}\mathcal{U}_{2\beta} \prod_{x\neq\alpha,\beta} \hat{a}^\dagger_x |\text{vac}\rangle\right] - \left[\sum_{\alpha<\beta} (-1)^{\alpha+\beta} \mathcal{U}_{1\alpha}\mathcal{U}_{2\beta} \prod_{x\neq\alpha,\beta} \hat{a}^\dagger_x |\text{vac}\rangle\right] \\ =&\sum_{\alpha>\beta} (-1)^{\alpha+\beta} (\mathcal{U}_{1\alpha}\mathcal{U}_{2\beta} - \mathcal{U}_{1\beta}\mathcal{U}_{2\alpha}) \prod_{x\neq\alpha,\beta} \hat{a}^\dagger_x |\text{vac}\rangle \qquad \text{(relabeling indices)}\end{aligned}$$

which is now a linear combination of mutually orthogonal states, so the second order approximation of the parity expectation is:

$$\langle \hat{P} \rangle = 1 - 2 \sum_{i_1} \sum_{\alpha} |\mathcal{U}_{i_1\alpha}|^2 + 4 \sum_{i_1<i_2} \sum_{\alpha<\beta} |\mathcal{U}_{i_1\alpha}\mathcal{U}_{i_2\beta} - \mathcal{U}_{i_1\beta}\mathcal{U}_{i_2\alpha}|^2 - \dots \, .$$

Before considering the N-th order term, let us consider the third order term:

$$\hat{d}_3\hat{d}_2\hat{d}_1 \prod_{\alpha} \hat{a}^\dagger_\alpha |\text{vac}\rangle = \sum_{\alpha\neq\beta\neq\gamma} (-1)^{\alpha+\beta+\gamma+f(\alpha,\beta,\gamma)} \mathcal{U}_{1\alpha}\mathcal{U}_{2\beta}\mathcal{U}_{3\gamma} \prod_{x\neq\alpha,\beta,\gamma} \hat{a}^\dagger_x |\text{vac}\rangle$$

where $f(\alpha,\beta,\gamma) = (\mathbb{1}_{\beta>\alpha} + \mathbb{1}_{\gamma>\alpha} + \mathbb{1}_{\gamma>\beta}) \mod 2$ by the same reasoning, where now the coefficients corresponding to all permutations of e.g. $\alpha,\beta,\gamma \in \{1,2,3\}$, i.e. 6 permutations, are factors of the same product state, so the sum is decomposed into 6 sums with indices $\alpha<\beta<\gamma, \alpha<\gamma<\beta, \dots$ with alternating minus signs for each permutation. One can work out that the third order approximation is now:

$$\hat{d}_3\hat{d}_2\hat{d}_1 \prod_{\alpha} \hat{a}^\dagger_\alpha |\text{vac}\rangle = \sum_{\alpha<\beta<\gamma} (-1)^{\alpha+\beta+\gamma} \left[\left(\sum_{\mathcal{P}} \text{sgn}_{\mathcal{P}} \mathcal{P}(\mathcal{U}_{1\alpha}\mathcal{U}_{2\beta}\mathcal{U}_{3\gamma}) \right) \prod_{x\neq\alpha,\beta,\gamma} \hat{a}^\dagger_x |\text{vac}\rangle \right]$$

where $\mathcal{P}(\mathcal{U}_{1\alpha}\mathcal{U}_{2\beta}\mathcal{U}_{3\gamma})$ denotes each of the six permutation of the α,β,γ indices and $\text{sgn}_{\mathcal{P}}$ the sign of the permutation. Again, we wrote the sum as a linear combination of mutually orthogonal Fock states. If we apply the same reasoning for the N-th terms, we obtain $N!$ permutations and the full parity expectation can be written as:

$$\begin{aligned}
\langle \hat{P} \rangle (t) =& 1 - 2 \sum_{i_1} \sum_{\alpha} |\mathcal{U}_{i_1\alpha}|^2 + 4 \sum_{i_1<i_2} \sum_{\alpha<\beta} |\mathcal{U}_{i_1\alpha}\mathcal{U}_{i_2\beta} - \mathcal{U}_{i_1\beta}\mathcal{U}_{i_2\alpha}|^2 \\
& - 8 \sum_{i_1<i_2<i_3} \sum_{\alpha<\beta<\gamma} |\mathcal{U}_{i_1\alpha}\mathcal{U}_{i_2\beta}\mathcal{U}_{i_3\gamma} - \mathcal{U}_{i_1\beta}\mathcal{U}_{i_2\alpha}\mathcal{U}_{i_3\gamma} + \mathcal{U}_{i_1\beta}\mathcal{U}_{i_2\gamma}\mathcal{U}_{i_3\alpha} - \dots|^2 \\
& + 16 \sum_{i_1<\dots<i_4} \sum_{\alpha<\dots<\delta} \left| \sum_{\mathcal{P}} \text{sgn}_{\mathcal{P}} \mathcal{P}(\mathcal{U}_{i_1\alpha} \dots \mathcal{U}_{4\delta}) \right|^2 - \dots \, .
\end{aligned}$$

2. Heisenberg picture

The alternative approach to the one used above is to include the unitary operators in the parity operator, similar to what we did with single particle operators. This approach was not developed in this thesis but we present it for future discussion. Consider the Heisenberg parity operator:

$$\begin{aligned}
\hat{P}(t) &= \hat{U}^\dagger(t) \cdot \prod_{\alpha\in[N]} (1 - 2\hat{d}^\dagger_\alpha \hat{d}_\alpha) \cdot \hat{U}(t) \\
&= \prod_{\alpha\in[N]} (1 - 2\hat{d}^\dagger_\alpha(t)\hat{d}_\alpha(t))
\end{aligned}$$

where $\hat{d}^\dagger_\alpha := \hat{U}^\dagger(t)\hat{d}^\dagger_\alpha\hat{U}(t)$ which was defined in (5.5). The sum in (5.5) may be written exclusively in the positive part of the spectrum:

$$\hat{d}^\dagger_\alpha(t) = \sum_{\beta\in[N]} \mathcal{R}_{\alpha\beta}\hat{d}^\dagger_\beta + \mathcal{R}_{\alpha,-\beta}\hat{d}_\beta \tag{7.5}$$

such that all terms here mutually anti-commute. The single particle expectation number $\hat{d}^\dagger_\alpha(t)\hat{d}_\alpha(t)$ of evolved particles can then be written by simply taking the product:

$$\hat{n}_\alpha(t) = \sum_{i,j>0} \big(\mathcal{R}_{\alpha i}\mathcal{R}^*_{\alpha j}\cdot \hat{a}^\dagger_i\hat{a}_j + \mathcal{R}_{\alpha i}\mathcal{R}^*_{\alpha -j}\cdot \hat{a}^\dagger_i\hat{a}^\dagger_j + \\ \mathcal{R}_{\alpha -i}\mathcal{R}^*_{\alpha j}\cdot \hat{a}_i\hat{a}_j + \mathcal{R}_{\alpha -i}\mathcal{R}^*_{\alpha -j}\cdot \hat{a}_i\hat{a}^\dagger_j\big).$$

Referring to the expansion of the parity product (7.1), each K-th order product term of the form $\hat{n}_{i_1}\hat{n}_{i_2}...\hat{n}_{i_K}$ where $\hat{n}_\alpha := \hat{d}^\dagger_\alpha(t)\hat{d}_\alpha(t)$ will expand into a sum of 4^K terms of combinations of $\hat{a}^\dagger_i, \hat{a}_i$. However, only a few of the 4^K terms have nonzero contribution. For example, in the case $K=3$ one example term would be of the form $\langle\Omega|\hat{a}_3\hat{a}^\dagger_1\hat{a}^\dagger_2\hat{a}_1\hat{a}_2\hat{a}^\dagger_3|\Omega\rangle$ which is clearly zero in the stationary ground state. The selection rule for the terms which are nonzero can be understood with Wick's theorem introduced below.

Wick's theorem for time-independent operators.

Wick's theorem allows one to simplify products of creation and annihilation operators in time-dependent or stationary problems. We consider the case with stationary operators. Let $\prod_{i=1}^{2K}\hat{\alpha}_i$ be an arbitrarily ordered product of K creation and K annihilation operators i.e. $\hat{\alpha}_i \in \{\hat{c}^\dagger_i, \hat{c}_i\}$ with $i = 1, ..., K$. Define a pair contraction:

$$\overbrace{\alpha_i\alpha_j} = \langle\hat{\alpha}_i\hat{\alpha}_j\rangle\,.$$

Then Wick's theorem states [56]:

$$\langle\hat{\alpha}_1\hat{\alpha}_2...\hat{\alpha}_{2P}\rangle = \overbrace{\alpha_1\alpha_2}\overbrace{\alpha_3\alpha_4}...\overbrace{\alpha_{2P-1}\alpha_{2P}} \\ + \overbrace{\alpha_1\alpha_2}\overbrace{\alpha_3\alpha_4}...\overbrace{\alpha_{2P-1}\alpha_{2P}} \\ + ...$$

for the vacuum expectation value, i.e. normal ordered terms are taken to have an expectation value of zero, where the right hand side contains all the possible pairwise contractions. Thus there exist $\binom{2K}{2}$ contractions, the large majority of which will be zero given fermionic commutation relations. Finally, interchanging contractions produces a sign η:

$$\overbrace{\alpha_i\alpha_j\alpha_k\alpha_l} = -\eta\ \overbrace{\alpha_i\alpha_k}\overbrace{\alpha_j\alpha_l}$$

where $\eta = 1$ for fermions and $\eta = -1$ for bosons.

After some algebra one realizes that an arbitrary product $\langle\hat{n}_1\hat{n}_2...\hat{n}_K\rangle$ can be written as a sum over $2K$ indices with 4^K terms. After applying Wick contractions, one is able to factorize the sums, where each sum groups the prefactors of a contracted pair. As contractions are only nonzero between an annihilation operator on the left and a creation operator on the right, the only terms that can be involved are the elements of the following matrix:

$$\Theta^{\alpha\beta} = \begin{pmatrix}\Theta^{\alpha\beta}_{00} & \Theta^{\alpha\beta}_{01}\\ \Theta^{\alpha\beta}_{10} & \Theta^{\alpha\beta}_{11}\end{pmatrix} \equiv \begin{pmatrix}\sum_{x\in[N]}\mathcal{R}_{\alpha -x}\mathcal{R}_{\beta x} & \sum_{x\in[N]}\mathcal{R}^*_{\alpha x}\mathcal{R}_{\beta x}\\ \sum_{x\in[N]}\mathcal{R}_{\alpha -x}U^*_{\beta -x} & \sum_{x\in[N]}\mathcal{R}^*_{\alpha x}\mathcal{R}^*_{\beta -x}\end{pmatrix}$$

Let us illustrate this with a second order term. For this case there exist three nonzero

terms:

$$\begin{aligned}\langle \hat{n}_\alpha \hat{n}_\beta \rangle &= \sum_{i,j,p,q\in[N]} \Big(\mathcal{R}_{\alpha-i}\mathcal{R}^*_{\alpha j}\mathcal{R}_{\beta p}\mathcal{R}^*_{\beta-q}(\overbrace{a_i a_j a_p^\dagger a_q^\dagger}^{} + \overbrace{a_i a_j a_p^\dagger a_q^\dagger}^{}) \\ &\qquad + \mathcal{R}_{\alpha-i}\mathcal{R}^*_{\alpha-j}\mathcal{R}_{\beta-p}\mathcal{R}^*_{\beta-q}(\overbrace{a_i a_j^\dagger}^{}\overbrace{a_p a_q^\dagger}^{}) \Big) \\ &= \sum_{i,j,p,q\in[N]} \Big(\mathcal{R}_{\alpha-i}\mathcal{R}^*_{\alpha j}\mathcal{R}_{\beta p}\mathcal{R}^*_{\beta-q}(\delta_{jp}\delta_{iq} - \delta_{ip}\delta_{jq}) + \mathcal{R}_{\alpha-i}\mathcal{R}^*_{\alpha-j}\mathcal{R}_{\beta-p}\mathcal{R}^*_{\beta-q}(\delta_{ij}\delta_{pq}) \Big) \\ &= \Theta^{\alpha\beta}_{01}\Theta^{\alpha\beta}_{10} - \Theta^{\alpha\beta}_{00}\Theta^{\alpha\beta}_{11} + \Theta^{\alpha\alpha}_{01}\Theta^{\beta\beta}_{01}\end{aligned}$$

where the sums corresponding to a respective contracted pairs were factorized in the last step and expressed in terms of $\Theta^{\alpha\beta}$. The entire procedure can be generalized in a computer program for higher order terms.

■ Chapter VIII
Conclusion

The proposal of Ref. [18] has opened a novel route towards the measurement of the parity of bulk vortices by exploiting the edges of the superconductor. Unlike most current alternatives, this proposal leaves the vortices completely unaffected by the measurement. In this thesis, it was demonstrated that the measurement of the quantized charge holds in a fully dynamical description even as the system does not return to the ground state manifold.

The BdG Hamiltonian was evolved in the absence and presence of bulk vortices – which were introduced by a separate calculation for the phase in the superconductor. The redundancies in the BdG theory were considered in evaluating expectation values of single-particle observables in the time-evolved many-body ground state, and the convergence of two basis decompositions in energy was studied. The theoretical predictions were found to hold despite the coupling of edge fermions with the bound states in the junction and they hold remarkably well in the presence of path-length differences. Fast injections of the edge-vortices have shown small oscillations in current density which integrate to at most 10% of the expected unit charge at the exit, for injection times as fast as $10a/v$. On the whole, this work has shed light on the collective nature of the edge-vortex excitation and on its relationship to the superconducting ground state under time-evolutions.

Finally, promising results were obtained towards the characterization of the edge-vortex as a good qubit by a dynamical calculation of the many-body parity operator. As a consequence, edge-vortices can potentially be braided sequentially, which opens the possibility for elaborate qubit manipulations on the edge-vortex in the future.

Bibliography

[1] C. Nayak, S. H. Simon, A. Stern, M. Freedman, and S. Das Sarma, "Non-Abelian anyons and topological quantum computation," *Reviews of Modern Physics*, vol. 80, pp. 1083–1159, Sept. 2008.

[2] C. Beenakker, "Search for non-Abelian Majorana braiding statistics in superconductors," *SciPost Physics Lecture Notes*, p. 15, Aug. 2020.

[3] C. Beenakker, "Search for Majorana Fermions in Superconductors," *Annual Review of Condensed Matter Physics*, vol. 4, pp. 113–136, Apr. 2013.

[4] A. Grabsch, Y. Cheipesh, and C. W. J. Beenakker, "Dynamical Signatures of Ground-State Degeneracy to Discriminate against Andreev Levels in a Majorana Fusion Experiment," *Advanced Quantum Technologies*, vol. 3, p. 1900110, Jan. 2020.

[5] S. Frolov, "Quantum computing's reproducibility crisis: Majorana fermions," *Nature*, vol. 592, pp. 350–352, Apr. 2021.

[6] M. Aghaee and et al., "InAs-Al Hybrid Devices Passing the Topological Gap Protocol," Nov. 2022. arXiv:2207.02472 [cond-mat].

[7] Z. Cao, S. Chen, G. Zhang, and D. E. Liu, "Recent progress on Majorana in semiconductor-superconductor heterostructures–Engineering and detection," June 2022. arXiv:2206.06916 [cond-mat].

[8] G. E. Volovik, "Fermion zero modes on vortices in chiral superconductors," *Journal of Experimental and Theoretical Physics Letters*, vol. 70, pp. 609–614, Nov. 1999.

[9] N. Read and D. Green, "Paired states of fermions in two dimensions with breaking of parity and time-reversal symmetries and the fractional quantum Hall effect," *Physical Review B*, vol. 61, pp. 10267–10297, Apr. 2000.

[10] A. Y. Kitaev, "Unpaired Majorana fermions in quantum wires," *Physics-Uspekhi*, vol. 44, pp. 131–136, Oct. 2001.

[11] G. Moore and N. Read, "Nonabelions in the fractional quantum hall effect," *Nuclear Physics B*, vol. 360, pp. 362–396, Aug. 1991.

[12] B. H. November, J. D. Sau, J. R. Williams, and J. E. Hoffman, "Scheme for Majorana Manipulation Using Magnetic Force Microscopy," May 2019. arXiv:1905.09792 [cond-mat].

[13] J. Alicea, Y. Oreg, G. Refael, F. von Oppen, and M. P. A. Fisher, "Non-Abelian statistics and topological quantum information processing in 1D wire networks," *Nature Physics*, vol. 7, pp. 412–417, May 2011.

[14] D. Aasen, M. Hell, R. V. Mishmash, A. Higginbotham, J. Danon, M. Leijnse, T. S. Jespersen, J. A. Folk, C. M. Marcus, K. Flensberg, and J. Alicea, "Milestones Toward Majorana-Based Quantum Computing," *Physical Review X*, vol. 6, p. 031016, Aug. 2016.

[15] Y. Wu, H. Jiang, J. Liu, H. Liu, and X. Xie, "Non-Abelian Braiding of Dirac Fermionic Modes Using Topological Corner States in Higher-Order Topological Insulator," *Physical Review Letters*, vol. 125, p. 036801, July 2020.

[16] C. K. McLauchlan and B. Béri, "Fermion-Parity-Based Computation and Its Majorana-Zero-Mode Implementation," *Physical Review Letters*, vol. 128, p. 180504, May 2022.

[17] Y. Cheipesh, "Anyonic, cosmic, and chaotic: three faces of Majorana fermions," *Doctoral Thesis - Casimir PhD Series*, 2022.

[18] C. Beenakker, P. Baireuther, Y. Herasymenko, I. Adagideli, L. Wang, and A. Akhmerov, "Deterministic Creation and Braiding of Chiral Edge Vortices," *Physical Review Letters*, vol. 122, p. 146803, Apr. 2019.

[19] P. Fendley, M. P. A. Fisher, and C. Nayak, "Edge states and tunneling of non-Abelian quasiparticles in the = 5 2 quantum Hall state and p + i p superconductors," *Physical Review B*, vol. 75, p. 045317, Jan. 2007.

[20] C. Beenakker, A. Grabsch, and Y. Herasymenko, "Electrical detection of the Majorana fusion rule for chiral edge vortices in a topological superconductor," *SciPost Physics*, vol. 6, p. 022, Feb. 2019.

[21] C. Beenakker and D. Oriekhov, "Shot noise distinguishes Majorana fermions from vortices injected in the edge mode of a chiral p-wave superconductor," *SciPost Physics*, vol. 9, p. 080, Nov. 2020.

[22] I. Adagideli, F. Hassler, A. Grabsch, M. Pacholski, and C. W. J. Beenakker, "Time-resolved electrical detection of chiral edge vortex braiding," p. 20, 2020.

[23] F. Hassler, A. Grabsch, M. J. Pacholski, D. O. Oriekhov, O. Ovdat, I. Adagideli, and C. W. J. Beenakker, "Half-integer charge injection by a Josephson junction without excess noise," *Physical Review B*, vol. 102, p. 045431, July 2020.

[24] G. Stefanucci, E. Perfetto, and M. Cini, "Time-dependent quantum transport with superconducting leads: A discrete-basis Kohn-Sham formulation and propagation scheme," *Physical Review B*, vol. 81, p. 115446, Mar. 2010.

[25] J. Weston, "Time-Resolved Dynamics of Josephson Junctions," in *Numerical Methods for Time-Resolved Quantum Nanoelectronics*, pp. 81–100, Cham: Springer International Publishing, 2017. Series Title: Springer Theses.

[26] J. Schulenborg, S. Krøjer, M. Burrello, M. Leijnse, and K. Flensberg, "Detecting Majorana modes by readout of poisoning-induced parity flips," Sept. 2022. arXiv:2209.08082 [cond-mat].

[27] W. Chen, J. Wang, Y. Wu, J. Qi, J. Liu, and X. C. Xie, "Non-Abelian statistics of Majorana zero modes in the presence of an Andreev bound state," *Physical Review B*, vol. 105, p. 054507, Feb. 2022.

[28] T. Sanno, S. Miyazaki, T. Mizushima, and S. Fujimoto, "*Ab initio* simulation of non-Abelian braiding statistics in topological superconductors," *Physical Review B*, vol. 103, p. 054504, Feb. 2021.

[29] L. Fu and C. L. Kane, "Probing Neutral Majorana Fermion Edge Modes with Charge Transport," *Physical Review Letters*, vol. 102, p. 216403, May 2009.

[30] D. A. Ivanov, "Non-Abelian Statistics of Half-Quantum Vortices in p -Wave Superconductors," *Physical Review Letters*, vol. 86, pp. 268–271, Jan. 2001.

[31] L. Fu and C. L. Kane, "Superconducting Proximity Effect and Majorana Fermions at the Surface of a Topological Insulator," *Physical Review Letters*, vol. 100, p. 096407, Mar. 2008.

[32] A. R. Akhmerov, J. Nilsson, and C. W. J. Beenakker, "Electrically Detected Interferometry of Majorana Fermions in a Topological Insulator," *Physical Review Letters*, vol. 102, p. 216404, May 2009.

[33] A. C. Potter and L. Fu, "Anomalous supercurrent from Majorana states in topological insulator Josephson junctions," *Physical Review B*, vol. 88, p. 121109, Sept. 2013.

[34] X.-L. Qi, T. L. Hughes, and S.-C. Zhang, "Chiral topological superconductor from the quantum Hall state," *Physical Review B*, vol. 82, p. 184516, Nov. 2010.

[35] J. Bardeen, L. N. Cooper, and J. R. Schrieffer, "Microscopic Theory of Superconductivity," *Physical Review*, vol. 106, pp. 162–164, Apr. 1957.

[36] Y. V. Nazarov and J. Danon, *Advanced quantum mechanics: A practical guide*. Cambridge New York: Cambridge University Press, 2013.

[37] R. M. Fernandes, "Lecture Notes: BCS theory of superconductivity," *Gleb Wataghin Institute of Physics – University of Campinas (UNICAMP), Brazil*, 2015.

[38] A. L. Fetter and J. D. Walecka, *Quantum theory of many-particle systems*. Mineola, N.Y: Dover Publications, 2003.

[39] N. Bogoliubov, "A new method in the theory of superconductivity," *Sov. Phys. JETP*, 1958.

[40] J. G. Valatin, "Comments on the theory of superconductivity," *Il Nuovo Cimento*, vol. 7, pp. 843–857, Mar. 1958.

[41] X.-L. Qi, Y.-S. Wu, and S.-C. Zhang, "Topological quantization of the spin Hall effect in two-dimensional paramagnetic semiconductors," *Physical Review B*, vol. 74, p. 085308, Aug. 2006.

[42] R. Aguado, "Majorana quasiparticles in condensed matter," *La Rivista del Nuovo Cimento*, vol. 40, pp. 523–593, Oct. 2017. arXiv:1711.00011 [cond-mat].

[43] A. Akhmerov, J. Sau, B. van Heck, S. Rubbert, R. Skolasiński, B. Nijholt, I. Muhammad, and T. Örn Rosdahl, "Bulk-edge correspondence in the Kitaev chain," *Online course on topology in condensed matter (topocondmat.org)*, 2015.

[44] A. A. Abrikosov, "Nobel Lecture: Type-II superconductors and the vortex lattice," *Reviews of Modern Physics*, vol. 76, pp. 975–979, Dec. 2004.

[45] M. A. Rashid, "Lecture notes: Superconductivity," *Jashore University of Science and Technology*, p. 8, 2019.

[46] R. Hlubina, "Lectures on Superconductivity," *Comenius University Bratislava*, 2016.

[47] P. W. Anderson, "Anomalous Magnetothermal Resistance of High-Tc Superconductors: Anomalous Cyclotron Orbits at a Dirac Point," Dec. 1998. arXiv:cond-mat/9812063.

[48] P.-G. d. Gennes, *Superconductivity of metals and alloys*. Advanced book classics, Reading, Mass: Advanced Book Program, Perseus Books, 1999.

[49] C. W. Groth, M. Wimmer, A. R. Akhmerov, and X. Waintal, "Kwant: a software package for quantum transport," *New Journal of Physics*, vol. 16, p. 063065, June 2014.

[50] R. Peierls, "On the Theory of the Diamagnetism of Conduction Electrons," *Zeitschrift für Physik*, vol. 80, no. 763-791, pp. 97–120, 1933.

[51] J. Weston, *Numerical methods for time-resolved quantum nanoelectronics*. Springer theses, recognizing outstanding Ph.D. research, Cham: Springer Nature, 2017.

[52] S. Datta and P. F. Bagwell, "Can the Bogoliubov–de Gennes equation be interpreted as a 'one-particle' wave equation?," *Superlattices and Microstructures*, vol. 25, pp. 1233–1250, May 1999.

[53] T. Kloss, J. Weston, B. Gaury, B. Rossignol, C. Groth, and X. Waintal, "Tkwant: a software package for time-dependent quantum transport," *New Journal of Physics*, vol. 23, p. 023025, Feb. 2021.

[54] J. Dormand and P. Prince, "A family of embedded Runge-Kutta formulae," *Journal of Computational and Applied Mathematics*, vol. 6, pp. 19–26, Mar. 1980.

[55] A. R. Akhmerov, "Topological quantum computation away from the ground state using Majorana fermions," *Physical Review B*, vol. 82, p. 020509, July 2010.

[56] A. L. Fetter, *Quantum Theory of Many-Particle Systems*. Dover Publications, 2012. OCLC: 868272360.